This is to certify that the

thesis entitled

The Composition of Impact Breccias
from the Chicxulub Impact Crater,
Yucatan Peninsula, Yucatan, Mexico

presented by

Catherine M. Corrigan

has been accepted towards fulfillment
of the requirements for

Masters degree in Geological Sciences

Major professor

Date 5/7/98

THE COMPOSITION OF IMPACT BRECCIAS FROM THE CHICXULUB IMPACT CRATER, YUCATÁN PENINSULA, YUCATÁN, MEXICO

By

Catherine M. Corrigan

A THESIS

Submitted to
Michigan State University
in partial fulfillment of the requirements
for the degree of

MASTER OF SCIENCE

Department of Geological Sciences

1998

ABSTRACT

THE COMPOSITION OF IMPACT BRECCIAS FROM THE CHICXULUB IMPACT CRATER, YUCATÁN PENINSULA, YUCATÁN, MEXICO

By

Catherine M. Corrigan

The Chicxulub impact crater, a 65 million year old impact crater centered on the northern coast of the Yucatan peninsula, Mexico, was formed by impact of an asteroid or comet into Tertiary sediments overlying a silicate basement.

This study examines the brecciated products of this impact to in order to determine more about their compositions and textures and how they are formed and emplaced. The majority of samples for this project came from the UNAM drill cores 5, 6 and 7. Samples from these cores were analyzed using X-ray Fluorescence, Electron Microscopy, petrologic microscopy and image analysis.

Breccias have been divided into two types based on the Ries Crater, Germany: those rich in deep target material containing textures associated with high shock (suevitic breccias), and those rich in CaO and MgO containing textures associated with lower shock temperatures (Bunte-type breccias).

The stratigraphy within the crater is inverted, with suevitic breccias overlying Bunte-type breccias. Inverted stratigraphy also exists within the U5 well and is exemplified by changing composition and texture with depth. The existence of suevitic breccias at a radial distance of 125 km and its absence at 150 km radius may place constraints on the crater's diameter of 250-300 km.

For my parents.

ACKNOWLEDGMENTS

I would like to thank my parents, grandparents and family, without whose encouragement and support I would never even have made it this far!

Thanks to my committee members, Dr. Buck Sharpton (without whom this project would never have existed!), Dr. Tom Vogel, Dr. Michael Velbel, Dr. Bill Cambray, and Dr. Duncan Sibley, for all of their guidance and support, both academically and financially.

I would especially like to thank the members of the Crisis Control Team, Dr. Ben Bussey, Wee Ann Feher, Laurel Pruski, Jeff Sisson, Dave "Pants" Szymanski, Karen Stockstill, Ed Wilson, Nate Mellott, room 114 Natural Science Bldg., all those who "could have been big" and the residents of the '97/'98 FOG House.

Special thanks to the Houston crew for their support and crazy times: Dr. Jeff Gillis, Leanne Woolley, David Gwynn, Mary Frybarger, Mary Sue Bell, the Martinez family (thanks for letting me stay!) and Yampa, Graham and Abigail Ryder, Mike Zolensky, Burkhard Dressler, Robbie Herrick and Carol Howard (thank for all of your help, Carol!!!).

Special thanks, again, to MAV, Mike Z, Buck and Dr. David Black for allowing me the opportunity to become involved in Planetary Geology in the first place.

TABLE OF CONTENTS

LIST OF TABLES

LIST OF FIGURES

INTRODUCTION

The 65 Ma Chicxulub Crater, Yucatan peninsula, Mexico (Figure 1,2), with a diameter of at least 200 km (and possibly over 300 km) is one of the largest recognized impact basins on the earth. Compared to the other two large, known impact structures, the Sudbury (~1.85 Ga, 140 km diameter) and Vredefort (~2 Ga, 160 km in diameter) structures, it is geologically young and relatively unmodified, making it an ideal area for study.

This study focuses on breccias deposited on the flanks of the Chicxulub impact crater. This material seems to land within approximately 2 crater radii from the center of crater, including within the transient crater. Any material landing outside of this transient crater is termed ejecta. The most important question addressed in this study is "how does this ejected material vary in composition and structure with distance from the crater's center?" Other relevant questions include: 1) What is the origin of this material? 2) How deep below the surface does the material originate? 3) How is it ejected and emplaced along the flanks of the crater? These questions will be addressed by evaluation of the nature and composition of impact breccias from three cores drilled by the Universidad Nacional Autonoma de Mexico (UNAM).

Previous Work

Because the large Chicxulub structure is buried beneath sediments and lacks topographic expression, it was discovered by gravity and magnetic

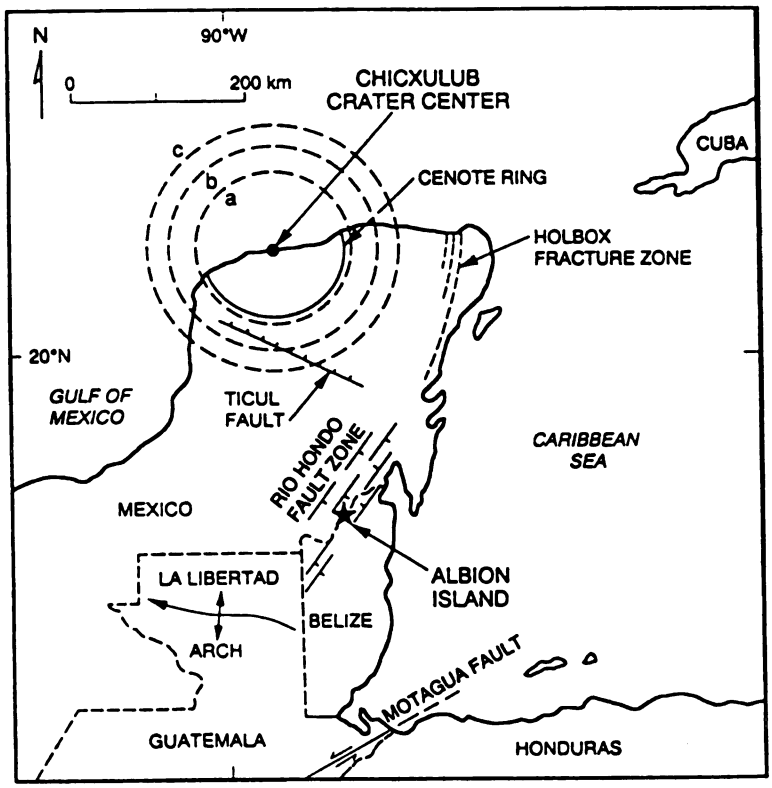

Figure 1. Map of the Gulf of Mexico area, showing the location of the Chicxulub impact crater (from Ocampo et al., 1996).

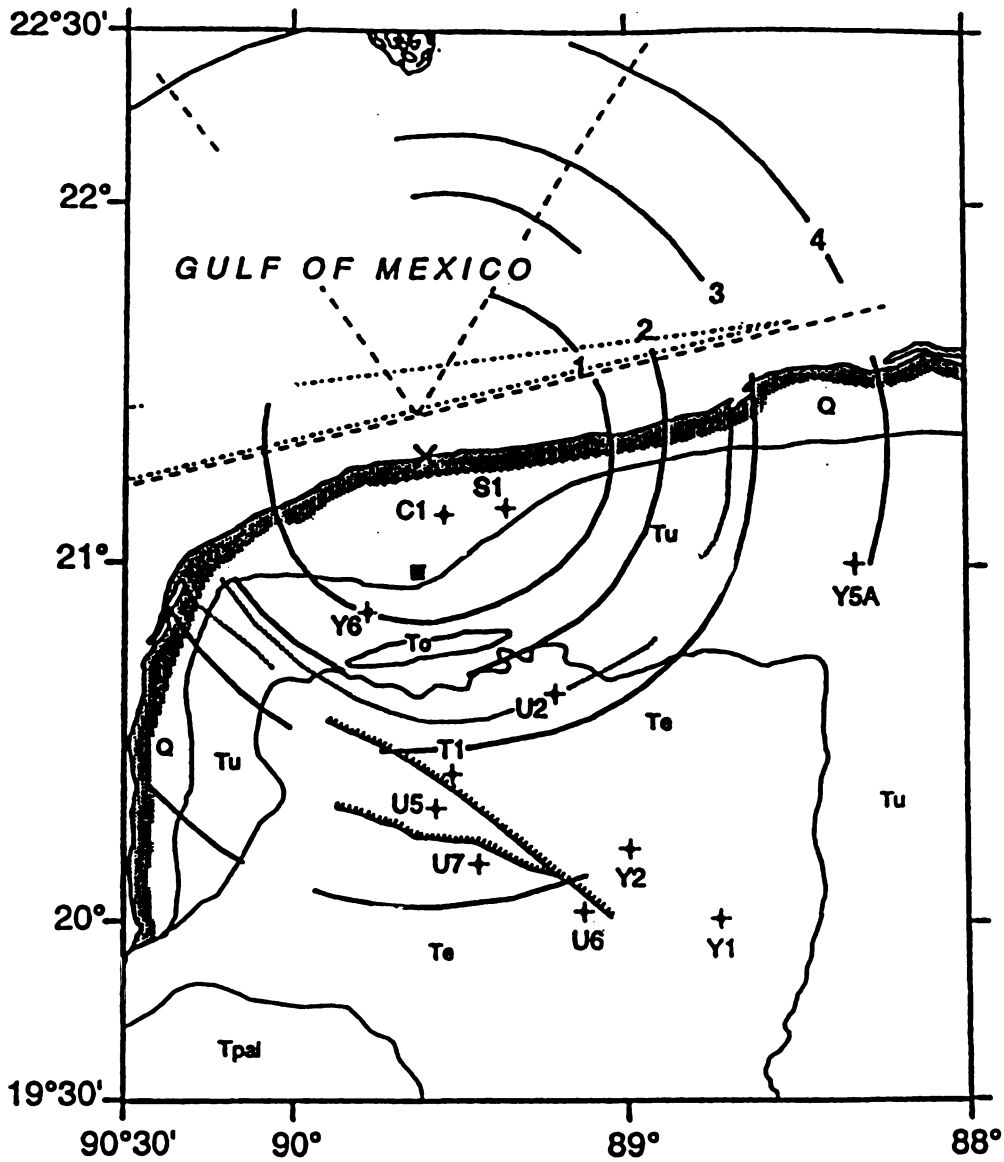

Figure 2. Close-up map of the Chicxulub impact crater showing the approximate location of crater rings. The center of the crater is represented by the X north of the city of Merida. Well locations are as marked (from Sharpton et al., unpublished).

methods. In the early 1950's, Petroleos Mexicanos (Pemex) drilled test wells into the structure. Unusual breccias and crystalline silicate rocks were intercepted in three of these wells. These breccias were originally interpreted to be of volcanic origin, but now most workers agree that they are ejecta deposits created by the collision of an extraterrestrial body (an asteroid, meteorite or comet) with the Earth (Hildebrand et al., 1991; Sharpton et al., 1992).

The Chicxulub basin has been linked to the Cretaceous / Tertiary (K/T) boundary by many methods. The ^{40}Ar-^{39}Ar ages of the melt rocks taken from the center of the crater reflect a melting/recrystallization age of 65 my (Izett et al., 1991; Swisher et al., 1992; Sharpton et al., 1992). Magnetic properties indicate that the basin was formed during a geomagnetic reversal period, which is consistent with the geomagnetics of the K/T boundary (magnetochron 29R; Sharpton et al., 1992; Urrutia-Fucugauchi et al., 1994). Melt rock compositions from the crater itself are the same as impact glass spherules in Haiti and NE Mexico, in terms of their isotopic properties, trace elements and major elements (Koeberl et al., 1994); and fragments of unmelted basement in breccia samples reveal a similar composition to shocked lithic fragments found at K/T sites worldwide (Sharpton et al., 1990). These shocked lithic fragments are believed to be impact induced. U-Pb determinations on zircons indicate that the age of the Chicxulub basement matches the age (545 Ma) of unmelted shock debris at the K/T boundary in Haiti and the western interior of North America (Krogh et al., 1993a, b; Bohor et al., 1993).

Craters that have three or more concentric rings (topographic or structural) are a class of impact features on planetary surfaces termed "multi-ringed impact basins." Examples of these include the Orientale Basin (Figure 3), which is located on the far side of the earth's moon (Spudis, 1993) and the Mead basin (Figure 4) of Venus (270 km diameter, located 12.5°N; 57.0°E), which may be the best planetary analog of the Chicxulub crater (Sharpton et al., 1997). Other than the Chicxulub crater, there are only two craters exceeding 150 km on Earth. These are the Sudbury structure in Ontario, Canada (Dressler et al., 1994), and the Vredefort structure in South Africa (Reimold, 1994), which are ~1850 Ma (Krogh et al., 1984) and ~2 Ma (Reimold, 1994), respectively. In contrast, Chicxulub is young and structurally unmodified. This gives us an excellent opportunity to study a young, unmodified feature of this magnitude. Very little is presently known about these features and the highly energetic collisions that form them. There is mounting evidence that the events creating such large features have the potential to bring about geological, biological and environmental change of global proportions (Sharpton et al., 1996) resulting in, for example, major extinction events such as that at near the Cretaceous/Tertiary boundary.

Ejecta studies have been conducted on other craters, and, though smaller in diameter, these can be of use in this investigation. Meteor Crater, Arizona, USA (Figure 5a), and the Ries Crater, Nördlingen, Germany, both approximately 1 km in diameter, have been examined in great detail. The ejected materials nearest to the rim of both craters possess an inverted

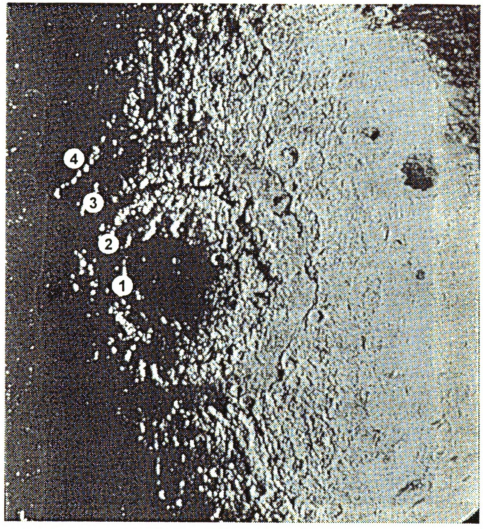

Figure 3. The lunar Orientale Basin and its concentric rings (from Spudis, 1993).

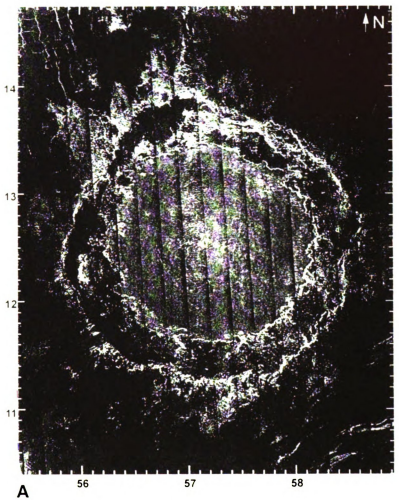

Figure 4. The Mead basin of Venus, which may be the best planetary analogue for the Chicxulub crater (from Sharpton et al., 1997).

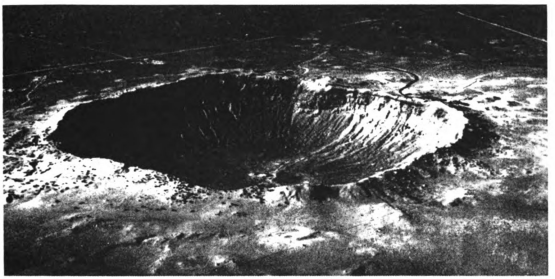

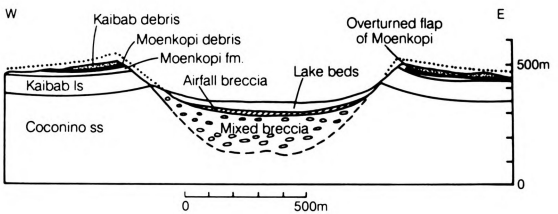

Figure 5a-b. a) An aerial view of Meteor Crater, Arizona (from Melosh, 1989);
b) This figures shows the overturned stratigraphy of Meteor Crater, Arizona (from Melosh, 1989).

stratigraphy, where an over-turned flap of older, deeper target material lies on top of younger, shallower target material (Melosh, 1989)(Figure 5b).

Purpose

This research proposes to closely examine the products of the Chicxulub impact by taking a close look at the chemistries and textures of impact breccias recovered from three wells drilled into the feature. Knowing something about the pre-existing stratigraphy of the area in question, it is possible to reconstruct, in a simplified manner, how that material may have been redistributed by the impact 65 million years ago. It is not known exactly what the compositions of the rocks within the structure are, or how they vary with distances from the center of the crater. Studying the ejecta from the Chicxulub crater in this and concurrent studies (Sharpton et al., unpublished) will aid greatly in the future understanding of this phenomenon by characterization not only of the breccias themselves, but of their vertical and lateral spatial variations around the crater.

Regional Geology

The Yucatan peninsula, has a complicated geologic history. It is now believed that before the late Paleozoic break-up of Pangea, the Yucatan block was positioned somewhere between the North American plate and the South American plate (Dietz and Holden, 1970), and was somewhat stretched in a north-northwest/ south-southeast direction during the breakup of this

supercontinent (Salvador, 1987, 1991). The original location of the peninsula is also unclear. Buffler and Sawyer (1985) indicate that it may have once been part of the South American plate. Salvador (1991) does not believe that any affinity exists between the Yucatan and the South American plate. He suggests, instead, a relation with the northeastern portion of Mexico, indicating that both have metamorphic sequences overlain by unmetamorphosed upper Paleozoic rocks intruded by Permian-Triassic granitic plutons. Salvador (1991) also notes that the possibility of the Yucatan having originally been a part of the North American continent still exists.

During the late Triassic to middle Jurassic, the Yucatan peninsula began to move away from the North American continent in the early rift stages of the Gulf of Mexico's formation (Pindell, 1985; Buffler and Sawyer, 1985). During this separation the area encountered stretching of anywhere from 470 km (Buffler and Sawyer, 1985) to 520 km (Pindell, 1985). This crustal extension (which, according to Salvador (1991), may represent 50-55% of the displacement of the Yucatan block) was accompanied by rotation of anywhere from 10 degrees (Salvador, 1987) to 50 degrees (Ross and Scotese, 1988) in a counterclockwise direction to 25 degrees in a clockwise direction (Hall, 1982). These values are dependent on where the authors place the Yucatan block during late Paleozoic to early Mesozoic time.

Movement during this time (late Triassic to middle Jurassic) most likely took place along transform boundaries, though where these were located is an unresolved issue. Salvador (1987) proposed that there existed two major

parallel rift zones trending N-NE/S-SW, one along the east coast of present-day Mexico and the other running the length of the modern-day Florida Escarpment. Pindell (1985) proposed a western transform fault, called the "Tamaulipas-Golden Lane-Chiapas" transform fault. This fault had a SW trend along the Chiapas massif. Buffler and Sawyer (1985), though not indicating a present-day location of the faults, suggested a western transform with a smaller transform in the southeastern Gulf of Mexico.

The movement along these faults and the accompanying rotations of the Yucatan block have Buffler and Sawyer (1985) and Salvador (1987) placing the block against the western Florida Platform during the existence of Pangea, and Pindell (1985) placing it farther west, against Texas and Louisiana.

During the early to late Jurassic, the Yucatan block had reached its current position east of southern Mexico where it remained an emergent landform, and was most likely still connected to the Florida Platform (Salvador, 1991) until the late Kimmeridgian. During the earliest Cretaceous, a major transgression occurred, and by the late Aptian or early Albian, the peninsula was covered by shallow water leading to the deposition of carbonates and evaporites in the area (Salvador, 1991). During the Cenomanian, the margin of the peninsula facing the deep portions of the Gulf of Mexico basin was dominated by reefs of rudist corals. During the mid-Cenomanian, a major unconformity exists along the margins of the platform, indicating a major lowering of sea level. By the end of the Cenomanian, the water level transgressed once again, but the platform edges were now bordered by open

marine shelves depositing carbonates, instead of corals and organic banks (Salvador, 1991).

At the end of the Cretaceous, the Yucatan peninsula was struck by an asteroid (or comet) of at least 10 km in diameter, and possibly as much as 15 km diameter, (Sharpton et al., 1996), throwing target material (ejecta) hundreds of kilometers laterally from the impact site. At the time of impact, three major compositional components of the target were in existence: 1) Upper Cretaceous limestones and dolostones, 2) Lower Cretaceous dolomites and anhydrites 3) Silicate basement (Sharpton, 1997). The region was covered by a shallow sea at the time of impact, possibly shielding the resulting basin, somewhat, from further erosion after formation. However, wave action has most likely intensely modified the high-standing rim and ejecta facies along the basin's flanks (Sharpton et al., 1996).

The center of the crater is located approximately 30 km north of Mérida, the capital city of Yucatán, Mexico (Figure 2), leaving the northern half of the crater buried not only by sediment, but by water. Since the end of the Cretaceous, the Yucatan peninsula has remained a stable area of shallow water carbonate and evaporite deposition (Salvador, 1991). The entire basin is now buried by up to a kilometer of Cenozoic sediments, which include limestones, dolostones, calcareous dolostones, and both calcareous and dolomitic shales (Sharpton, 1997).

The only easily recognizable topographic indicators of the crater include an arc of water-filled sinkholes (termed cenotes) located ~80 km from the

crater's center (Figure 2), that lie across the northwest edge of the Yucatán peninsula. There is a possibility that topographic evidence of a crater ring is in existence (Sharpton, 1997)(Figure 6). This ring, which would be the basin's fourth structural ring, is located farther out from the center of the crater than the ring of cenotes, and if verified, will be the only surface effect of a structural ring known to exist from the Chicxulub crater.

Methods

The study of impact craters on Earth is extremely important to the understanding of the impact processes that have operated in our Solar System since its birth. Though small scale craters like Meteor Crater in Arizona and the Ries Crater in Germany are well understood, the mechanics of large impact events remain unclear, despite much research in the field. Studying the Chicxulub impact crater may better enable us to constrain the events that take place during large scale impact, especially that of ejecta origin and subsequent emplacement. On a smaller scale, little is known about the actual composition of the rocks (breccias) in question.

This study consists of a combination of numerous analytical methods. Breccia samples from the Chicxulub impact structure, obtained from logged cores at various distances from the crater's center, were analyzed to determine major and trace element compositions. This was done using X-ray fluorescence spectrometry (XRF) conducted at Michigan State University, Electron Microprobe (EMP) conducted at the NASA Johnson Space Center, and

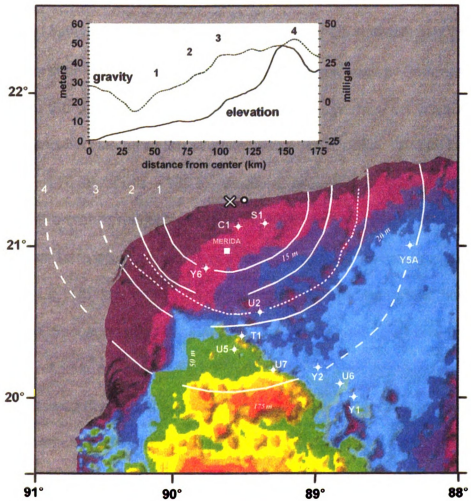

Figure 6. Topographic map of the Yucatan peninsula, Mexico, showing the possible topographic evidence of a fourth ring corresponding to the Chicxulub crater (from Sharpton et al., 1997).

image processing techniques for petrographic thin sections developed for this project conducted both at the Lunar and Planetary Institute and Michigan State University.

The samples used in this study originate from a combination of cores drilled by the Universidad Nacional Autonoma de Mexico (UNAM) and the Pemex Corporation, Mexico City, Mexico (the "Yucatan" wells). Samples were obtained from the cores listed in (Table 1), focusing primarily on three wells (UNAM 5, 6 and 7) drilled into the southern flank of the basin. These wells lie at distances of ~110 km south, ~150 km south-southeast and ~125 km south of the center of the crater, respectively (Figure 2). These samples will be discussed from here on in the order of their increasing distance from the center of the crater (i.e., U5, U7, U6). The samples from the Yucatan wells, however, will always be discussed after the UNAM wells, as they are not the main focus of this study. Additional samples were taken from the remaining cores as availability allowed (for example, Pemex core samples of breccias from the Y6 well, and basement rock samples from the Pemex cores Y1 and Y2).

The sampling strategy undertaken involved the selection of samples from the above listed cores in a manner that focused mainly on the U5 well. This afforded us the ability to assess, in detail, the variations within this well, and make general comparisons with the chemical variations in samples from other wells, particularly with respect to variations with radial distance from the center of the crater. Selection efforts focused primarily on matrix-rich breccias lacking clasts of significant size (>~1-2 cm)(Appendix A), as avoidance of large

Table 1. Description of wells, including their sites, depths, surface geologies and other comments (from Sharpton et al., unpublished).

Well Site	Depth, Surface Geology	Objectives, Comments
UNAM 1; southeast of center on innermost prominent gravity ring (Sharpton *et al.*, 1993); distance from basin center: ~50 km). See Figure C1.	200 m T.D. Eocene-Oligocene carbonates; ~85% core recovery.	attempted to core ~600 m to understand basin filling evolution near center. Drilling terminated when loss of circulation and continued caving could not be remedied
UNAM 2.; ~85 km southeast of center on 'ring of cenotes' (Pope *et al.*, 1991). Corresponds to proposed rim in Hildebrand *et al.* (1991) and Pilkington and Hildebrand (1994) model. Corresponds approximately to modified transient crater boundary in Sharpton *et al.* (1993) model. See Figure C1.	560 m T.D. Eocene carbonates; ~85% core recovery.	assess origin of ring of cenotes and link with crater. Constrain basin size, depth and infilling history; evaluate proposed crater models and kill mechanisms; document impact breccia characteristics at this site. T.D. did not reach crater at this site.
UNAM 3; east of center just inside gravity ring 4 (Figure C1), proposed rim of Sharpton *et al.* (1993).	70 m T.D. Eocene carbonates; ~65% core recovery.	lost circulation, caving; terminated coring
UNAM 4; just south of U3 (Figure C1), on the proposed rim of Sharpton *et al.* (1993).	125 m T.D. Eocene carbonates. ~70% core recovery	lost circulation, caving; terminated coring
UNAM 5; ~110 km south of center on ring 3 at Santa Elena (Figure C1). Proposed rim in Sharpton *et al.* (1993).	503 m T.D. impact melt encountered at 330 m; suevitic crystalline rock clast breccia at ~360 m to T.D..	constrain basin size, depth, and infilling history; evaluate crater models, kill mechanism(s), and impact breccia characteristics at this site
UNAM 6; ~150 km SSE of center on ring 4 near Peto.	~702 m T.D.; carbonate-anhydrite-rich breccia to TD	ditto
UNAM 7; ~125 km south of center between rings 3 and 4 near Tekax.	~700 m T.D. Suevite breccia and underlying carbonate-anhydrite-rich impact breccia	ditto

clasts during sampling reduced the chances of encountering a compositional bias error during the determination of chemical composition. Twenty-two samples were selected for chemical analysis. Detailed descriptions of each hand sample can be found in Appendix A. Photographs of representative hand samples of breccias from each well can also be found in Appendix A.

X-ray fluorescence (XRF) spectrometry was conducted to determine the concentrations of major elements and selected trace elements in the breccias. This process involved measuring 1.0 gram splits of very finely ground rock powder, to which was added 9.0 grams of Lithium Tetraborate (for flux) and 0.16 grams of Ammonium Nitrate (to ensure oxidation). The materials were mixed together within platinum crucibles and then heated until they had melted. The melt was agitated for at least 20 minutes to ensure complete homogenization. Upon completion of this process, these melts were then poured into platinum molds and quenched, forming glass disks.

The twenty-two samples were analyzed for both major and trace element compositions in the XRF spectrometer at Michigan State University, East Lansing, Michigan, USA. The detection limits (Table 2) and standard deviations (Table 3) for the trace elements as well as the trimmed mean and standard deviations based on 16 repetitions for each major element are those reported in Table 2 of Mills et al. (1997) and Table 4 here.

The image processing technique developed (at the Lunar and Planetary Institute (LPI), Houston, Texas, USA) for the purpose of this project involved scanning petrographic thin sections into a Kodak photographic slide scanner

Table 2: Detection Limits (ppm) for glass disks for trace elements.

Element	Glass Disks
Ba	100 ppm
La	48
Cr	63
Ni	25
Zn	14
Rb	13
Sr	12
Y	14
Nb	15
Zr	14
Cu	40

Table 3: Relative standard deviations (%) for glass disks for trace elements.

Element	Glass Disks
Ba	10%
La	10
Cr	5
Ni	4
Zn	6
Rb	6
Sr	5
Y	6
Nb	6
Zr	6
Cu	6

Table 4: Statistical Data for Major-element Analyses on Two Standards Treated as Unknowns.

USGS BCR-1

(n=18)

Oxide	MSU	Std. Dev.	Given
SiO_2	54.81	0.127	54.11
TiO_2	2.26	0.009	2.24
Al_2O_3	13.74	0.071	13.64
FeO	12.26	0.032	12.11
MnO	0.18	0.005	0.18
MgO	3.50	0.011	3.48
CaO	6.99	0.012	6.65
Na_2O	3.26	0.018	3.27
K_2O	1.71	0.002	1.69
P_2O_5	0.36	0.005	0.36

USGS W-1

(n=16)

Oxide	MSU	Std. Dev.	Given
SiO_2	52.73	0.106	52.51
TiO_2	1.08	0.009	1.07
Al_2O_3	15.02	0.077	15.01
FeO	10.00	0.030	10.16
MnO	0.18	0.004	0.17
MgO	6.63	0.018	6.62
CaO	10.91	0.014	10.99
Na_2O	2.18	0.018	2.16
K_2O	0.64	0.002	0.64
P_2O_5	0.14	0.005	0.13

at 1200 dots-per-inch (dpi) resolution in sleeves of polarizing film, both crossed and uncrossed. Each image was then reduced to 900 (dpi) resolution to allow easier handling and manipulation of the images. Each image was then printed on a on a typical desktop 720-dpi printer and for future analysis. Analysis consisted of point counting: A gridded piece of mylar (with 0.25 inch grid cells) was placed over each image descriptions were recorded of materials located beneath each of the grid intersections. Point counting results are summarized in Table 5. In conjunction with standard petrographic analysis conducted both at the LPI and at Michigan State University to determine the different types of minerals, matrix and clasts present, this technique was used to aid in the determination of the distribution of different target materials as clasts during the emplacement of ejecta upon impact, as well as in the determination of the proportions of melt to clasts to matrix involved in the different types of breccias. The method of choosing thin sections for analysis involved the selection of representative samples of the rocks in each well. Two sections are excluded from this rule (U5-383-2a and U5-420-b), in that they were chosen because of the larger clasts within them for Electron Microprobe analysis. These were point counted only for comparative reasons.

Electron Microprobe analysis involved obtaining spot analyses of individual grains as points, as well as construction of elemental maps of an entire region of a thin section to obtain a better view of elemental variation within the selected area. Microprobe work was conducted at NASA's Johnson Space Center, located in Houston, Texas, USA on a Cameca SX-100 Electron

Table 5: Modal point count analysis shown in percent.

Component	U5-360	U5-365	U5-383-2A	U5-400	U5-420	U5-450	U5-483	U7-335	U6-302
CAVITY	1.28	1.60	0.00	3.94	1.60	0.85	1.30	0.58	0.00
CARBONATE	3.93	7.09	10.16	6.47	1.30	0.68	4.17	1.63	0.00
EVAPORITE	3.63	1.20	0.39	1.92	0.00	1.88	6.48	0.00	0.00
ANHYDRITE	0.00	0.00	0.00	0.00	0.86	0.00	2.22	5.98	0.00
GYPSUM	0.00	0.00	0.00	0.00	0.00	0.00	0.00	0.00	31.05
REACTION RIM	6.19	0.00	2.26	5.25	0.00	4.53	0.00	0.00	0.00
MELT/ALTERED MELT	9.14	12.48	6.01	20.65	20.22	26.30	21.67	26.21	0.00
MATRIX MAJORITY	44.60	70.36	16.90	55.21	52.86	65.76	61.76	54.62	68.95
MATRIX MINORITY	31.24	7.29	0.00	6.56	0.00	0.00	0.00	2.64	0.00
SILICATE CLAST	0.00	0.00	62.53	0.00	23.14	0.00	0.00	0.00	0.00
ANHYDRITE CLAST	0.00	0.00	0.00	0.00	0.00	0.00	0.00	8.55	0.00
OPAQUES	0.00	0.00	0.72	0.00	0.00	0.00	0.00	0.00	0.00
UNKNOWN	0.00	0.00	0.00	0.00	0.00	0.00	2.41	0.00	0.00

Microprobe. Elemental maps of two areas of the thin section U5-420 were analyzed in order to determine small-scale changes in matrix compositions. These maps can be seen in Appendix D.

Once chemical and modal compositions of the breccias were determined, the results were examined for variations between well sites, and, therefore, variations between distances from the center of the crater, as well as in variations in depths within each well. We then used these data to better constrain how deeply the crater was excavated and where the material was emplaced.

Whole Rock Chemical Compositions of Chicxulub Impact Breccia

Two types of Chicxulub impact breccia

The Chicxulub impact basin consists of two distinct breccia types. These include the suevitic breccias and the Bunte-type breccias after those found at the Ries Crater, Nördlingen, Germany (Sharpton et al., 1996; Hörz et al., 1982). The major differences between the two types of breccia lie in the components of their chemical makeup and their mechanisms of emplacement.

Suevitic breccias contain high abundances of SiO_2 and Al_2O_3, and relatively low values of CaO and MgO. Many of the clasts incorporated into these breccias consist of melted target materials and glass generated on impact. These breccias are what are termed allogenic breccias, in that they are deposited within rim of the crater upon formation. This type of breccia is

predominantly primary ejecta material, derived from deep crystalline targets (Corrigan, et al., 1997). There is only a very small representation of the platform sequence material in these breccias.

Bunte Breccias are those from an impact that are predominantly composed of the sedimentary portion of the target strata (Hörz, 1982). Bunte-type breccias contain a much lower abundance of SiO_2 and Al_2O_3 and a much higher abundance of CaO and MgO than the suevitic breccias. According to Sharpton et al. (1996), this type of breccia represents the continuous ejecta deposit of the Chicxulub crater. Most of the material in these breccias is representative of the platform sequence portion of the target. Little silicate basement material has been incorporated, although according to Sharpton et al. (1996), this lack of silicate representation may result from "chemical alteration and secondary mineralization working on the highly vulnerable shocked and partially melted basement clasts."

Major and trace element chemical compositions

Major elements

A total of 22 chemical analyses were performed on the Chicxulub impact breccias. The major and trace element analyses from XRF spectroscopy are given in Tables 6 and 7 of Appendix B. XRF techniques are discussed on page eight. Because of the loss of volatile compounds such as CO_2 and SO_4 during sample preparation, the data have been normalized to 100% (by weight) and all

of the following values are normalized values. There is a distinct variation in the chemical signatures of the Chicxulub impact breccias (Figure 7). Of the three main cores studied (U5, U6 and U7) wells U5 (high SiO_2 and low CaO) and U6 show distinct chemical signatures (low SiO_2, high CaO). The U7 well shows a combination of the two signatures of from U5 and U6 (Figure 7) possibly separated stratigraphically (Corrigan et al., 1997).

The major element trends in the 13 analyzed U5 samples exhibit high SiO_2 and Al_2O_3, with normalized values ranging from ~35 to ~56 and ~8 to ~14 wt.%, respectively. Low CaO and MgO values exist, ranging from ~10 to ~40 and ~3 to ~11 wt.%, respectively. As well depth increases (from 360 to 490 m) there appears to be a decreasing trend in SiO_2 (Figure 8), Al_2O_3 (Figure 8), K_2O, and other major oxides (Table 6, Appendix B), with the exception of CaO, which increases with depth (Figure 8), and MgO, which exhibits no real trend with increasing depth (Figure 8). The data presented here indicate that the U5 breccias are similar to the suevitic type breccias of the Ries Crater. These data are supported by XRF data of the same breccias from Sharpton et al. (unpublished) (Figure 9).

In order to compare data sets, all data from the Sharpton et al. (unpublished) set have also been normalized to 100%. Comparisons of same depth values between the two data sets can be seen in Table 8 and Figure 12. All iron data from both sets have been converted to FeO. These corrections can be seen in Table 9.

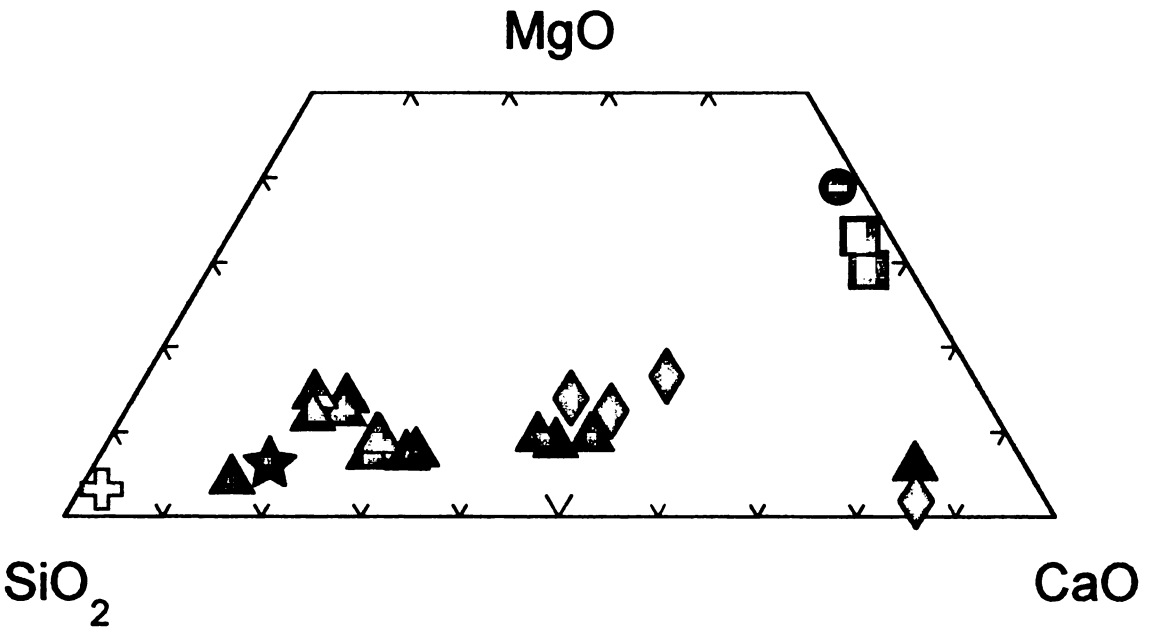

Figure 7. Ternary diagram of XRF data from Chicxulub impact breccias. Triangles = U5 samples; diamonds = U7 samples, squares = U6 samples; cross = Y6 sample; star = Y4 sample and circle = Y1 sample.

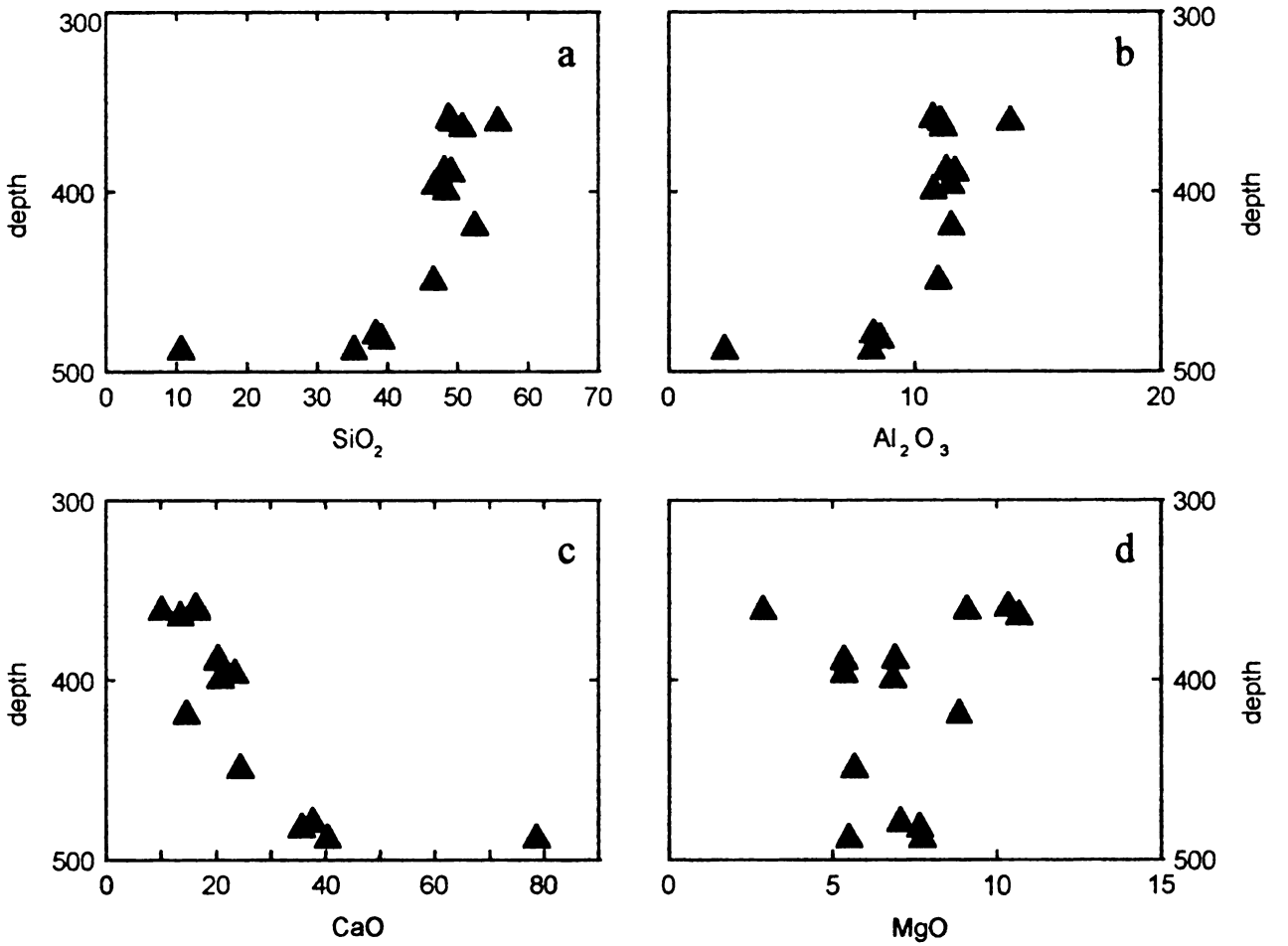

Figure 8a-d. Variations of composition with depth in the U5 well.

Figure 9a-c. Ternary diagrams comparing the data from this study (a) and that from Sharpton et al. (unpublished) (b): The large ternary diagram (c) shows the fields of data from the Sharpton et al. (unpublished) data overlain on the data from this study showing the two distinct trends that exist in the data.

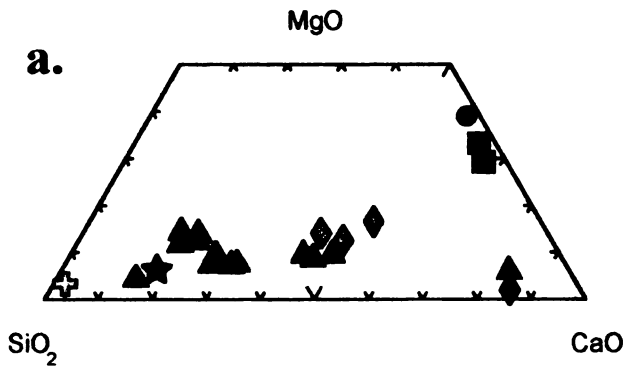
a.
MgO
SiO2
CaO

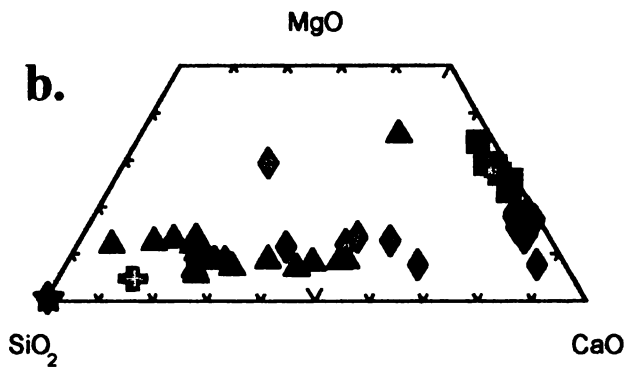
b.
MgO
SiO2
CaO

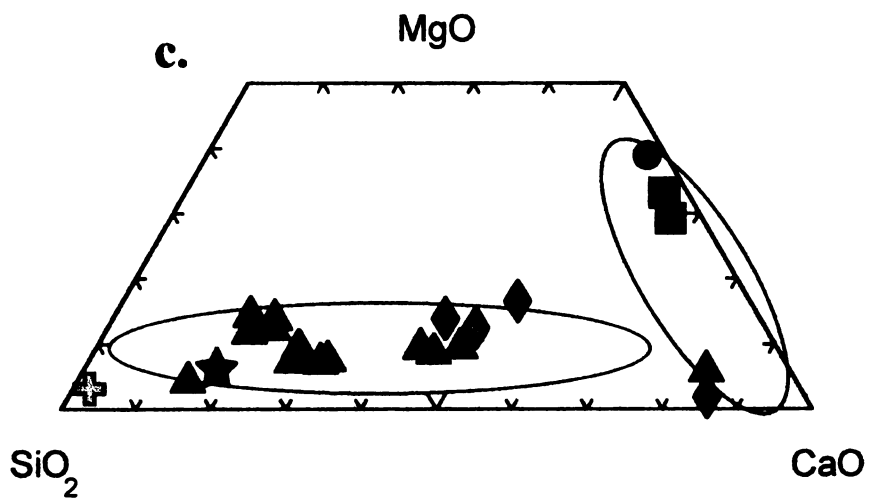
c.
MgO
SiO2
CaO

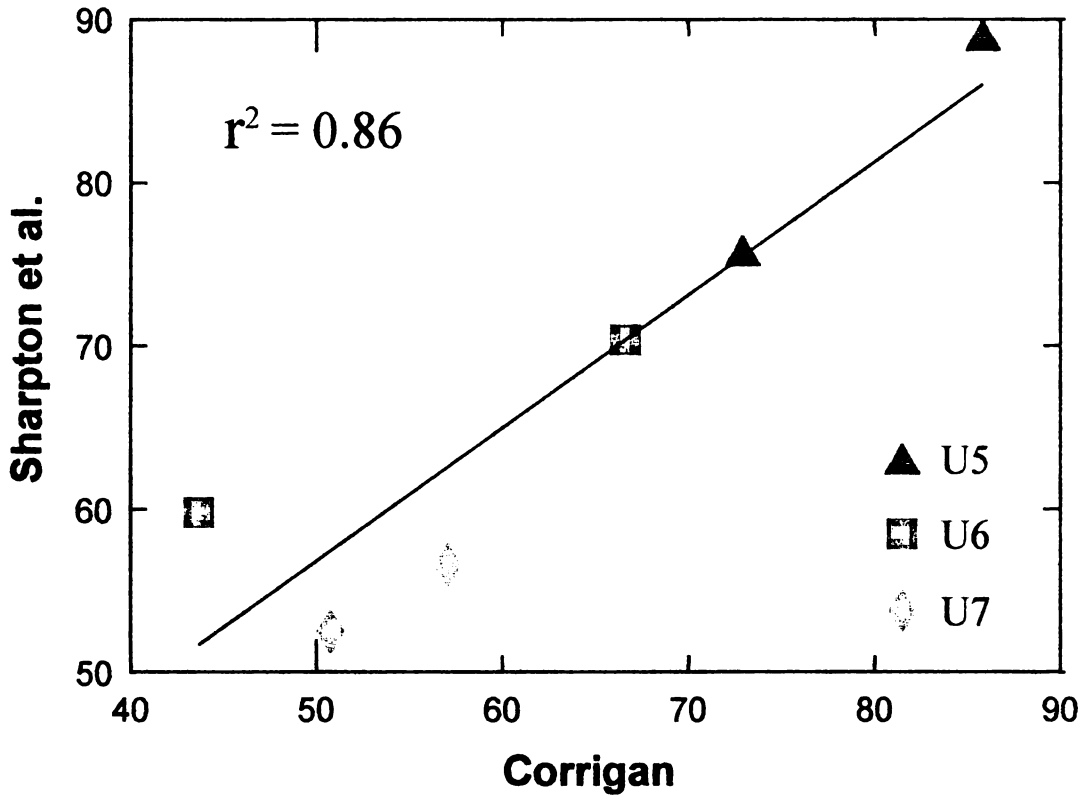

Figure 10. Plot of samples from this study against samples of the same wells and depth intervals from the Sharpton et al. (unpublished) data set to show correlations.

Table 8: Comparison of samples from this study (those followed by "C") and Sharpton et al. (unpublished).

Sample	SiO_2	Al_2O_3	MnO	MgO	CaO	Na_2O	K_2O	P_2O_5	TiO_2	FeO
U5-389-C	48.04	11.35	0.07	6.92	20.41	2.91	5.03	0.12	0.49	6.32
U5-389	52.48	9.75	0.06	5.78	17.23	2.39	3.69	0.02	0.38	0.00
U5-480-C	38.32	8.35	0.07	7.08	37.73	3.47	1.70	0.05	0.30	5.49
U5-480	40.05	7.16	0.07	5.88	33.37	2.81	1.33	0.00	0.23	0.00
U6-302-C	4.14	0.79	0.00	28.42	65.00	0.87	0.41	0.02	0.04	1.22
U6-302	3.91	0.35	0.00	17.89	41.14	0.04	0.14	0.00	0.02	0.00
U6-508-C	3.14	0.46	0.00	32.70	62.99	0.28	0.18	0.02	0.02	0.70
U6-508	2.97	0.16	0.00	19.93	37.22	0.04	0.06	0.00	0.02	0.00
U7-318-C	33.18	7.21	0.05	10.75	42.22	1.89	1.40	0.06	0.33	6.57
U7-318	27.97	5.94	0.04	8.66	36.16	1.41	1.06	n.d.	0.24	0.00
U7-699-C	12.52	1.85	0.00	1.81	81.46	0.64	1.01	0.02	0.09	3.12
U7-699	4.54	0.05	0.00	6.66	75.35	0.01	0.22	0.00	0.04	0.00

Table 9: Conversions of data from Sharpton et al. (unpublished) from Fe_2O_3 to FeO.

Sample	wt % Fe_2O_3	conversion factor	wt % FeO
U5-389	4.24	*.8998	3.82
U5-480	2.44	*.8998	2.20
U7-318	2.19	*.8998	1.97
U7-699	0.09	*.8998	0.08
U6-302	0.11	*.8998	0.10
U6-508	0.07	*.8998	0.06

The major element trends in the 4 analyzed samples from U7 exhibit a wide range of values. The normalized SiO_2 and Al_2O_3 values vary from ~12 to ~35 and ~2 to 8 wt.% respectively, and the CaO and MgO values vary from 37 to 81 and 2 to 14 wt.% respectively. The variation in these abundances show a break in the types of breccias that exist (Figure 7). This is verified by the XRF data from Sharpton et al. (unpublished)(Figure 9). The data presented in Appendix B suggests that both the suevitic and Bunte type breccias exist in the U7 well.

The major element concentrations in the two U6 samples analyzed exhibit very similar proportions of elemental abundances. SiO_2 and Al_2O_3 are low (3 and 4 wt. %) (Figure 7) and when compared with the XRF data from Sharpton et al. (unpublished) it seems that they remain low throughout the depth of the core (302 to 508 m)(Figure 9). CaO (with values of 3 and 65 wt. %) and MgO (with values of ~33 and 28 wt.%) are abundant and fairly constant and remain so throughout the core (Table 6, Appendix B). It appears from the data presented here that the U6 breccias are similar to the Bunte-type breccias of the Ries Crater.

The three samples analyzed from the Yucatan wells Y1, Y2 and Y6 all exhibit very high proportions of SiO_2 and lower abundances of Al_2O_3, CaO, and MgO. These data are also supported by those from Sharpton et al. (unpublished)(Figure 9).

On a ternary plot with SiO_2, MgO and CaO as the end members (Figure 7), most of the U5 samples fall in the high SiO_2, low MgO, low CaO range, with

a few of the deeper samples falling in a range of almost 50% CaO. These samples are from the bottom of the well (Figure 8). One sample from the well falls in the very low SiO_2, very high CaO range. This sample is thought to be a representative of a carbonate clast within the silicate matrix. On the same plot, samples from the U7 well are divided into two areas; those samples that fall near the deeper samples from the U5 well, and one that falls near the high CaO sample from U5. The U6 samples plot in the very low SiO_2 range, with intermediate amounts of both CaO and MgO.

General trends from these data follow. On a ternary plot of K_2O, SiO_2 and CaO (Figure 10), only those samples from the upper portion of the U5 well show an increase in K_2O concentrations. Figure 11-a shows a plot of MgO vs. CaO+MgO. This plot shows two trends, a low CaO+MgO trend and a high CaO+MgO trend. Notice that samples from U7 fall on both trends. Na_2O and K_2O abundances tend to increase with increasing SiO_2 as seen in Figure 11-b. TiO_2 exhibits an increase in abundance with increasing SiO_2 (Table 6), and a decrease in abundance with CaO+MgO (Figure 13).

Trace elements

The trace element trends from the Chicxulub impact breccias are shown in Table 7 of Appendix B. Apparent trends are as follows. Figure 14-b shows Zr decreasing with depth in the U5 well, while Figure 14-a shows Zr increasing in abundance with increasing SiO_2. Sr shows an increase in abundance with

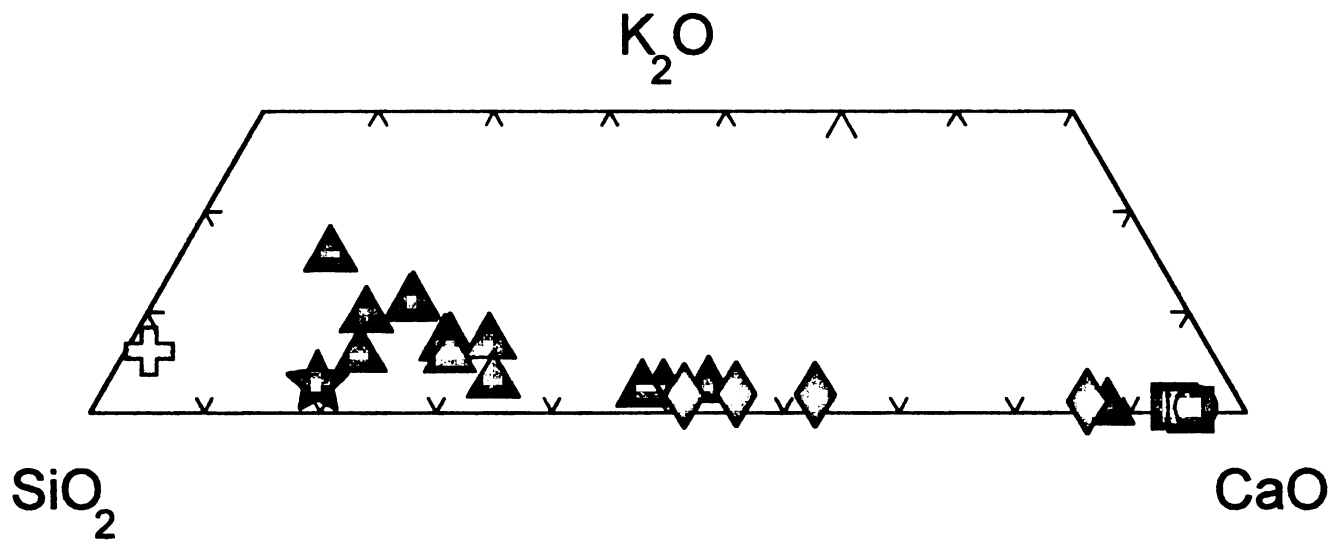

Figure 11. Ternary plot of XRF data showing variations in K_2O with CaO and SiO_2. Triangles = U5 samples; diamonds = U7 samples; squares = U6 samples; cross = Y6 sample; star = Y4 sample and circle = Y1 sample.

Figure 12a-b. Plots of XRF data: a) MgO vs. CaO + MgO showing the two distinct trends that exist in the data; b) $Na_2O + K_2O$ vs. SiO_2. Symbols for both figures are as follows: triangles = U5 samples; diamonds = U7 samples; squares = U6 samples; cross = Y6 sample; star = Y4 sample and circle = Y1 sample.

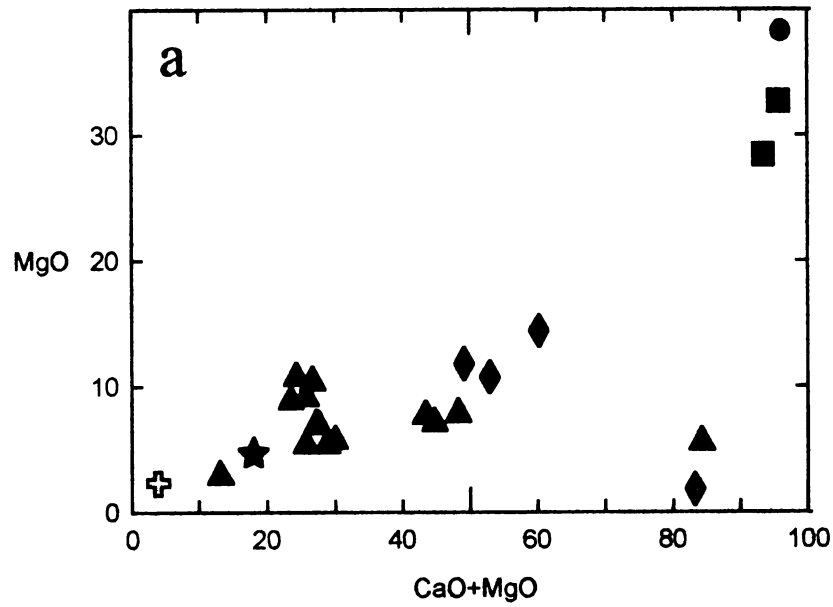
a
MgO
30
20
10
0
0
20
40
60
80
100
CaO+MgO

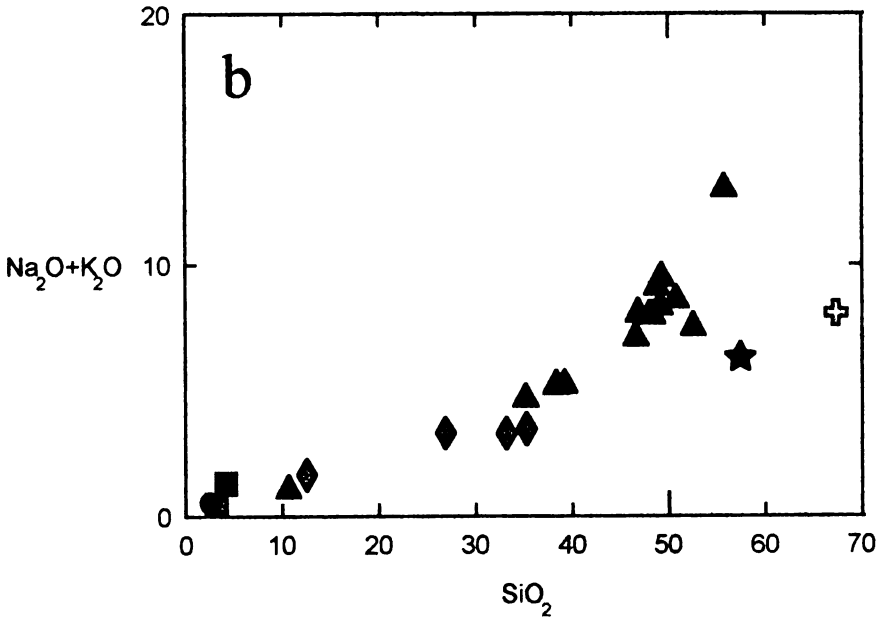
b
Na2O+K2O
20
10
0
0
10
20
30
40
50
60
70
SiO2

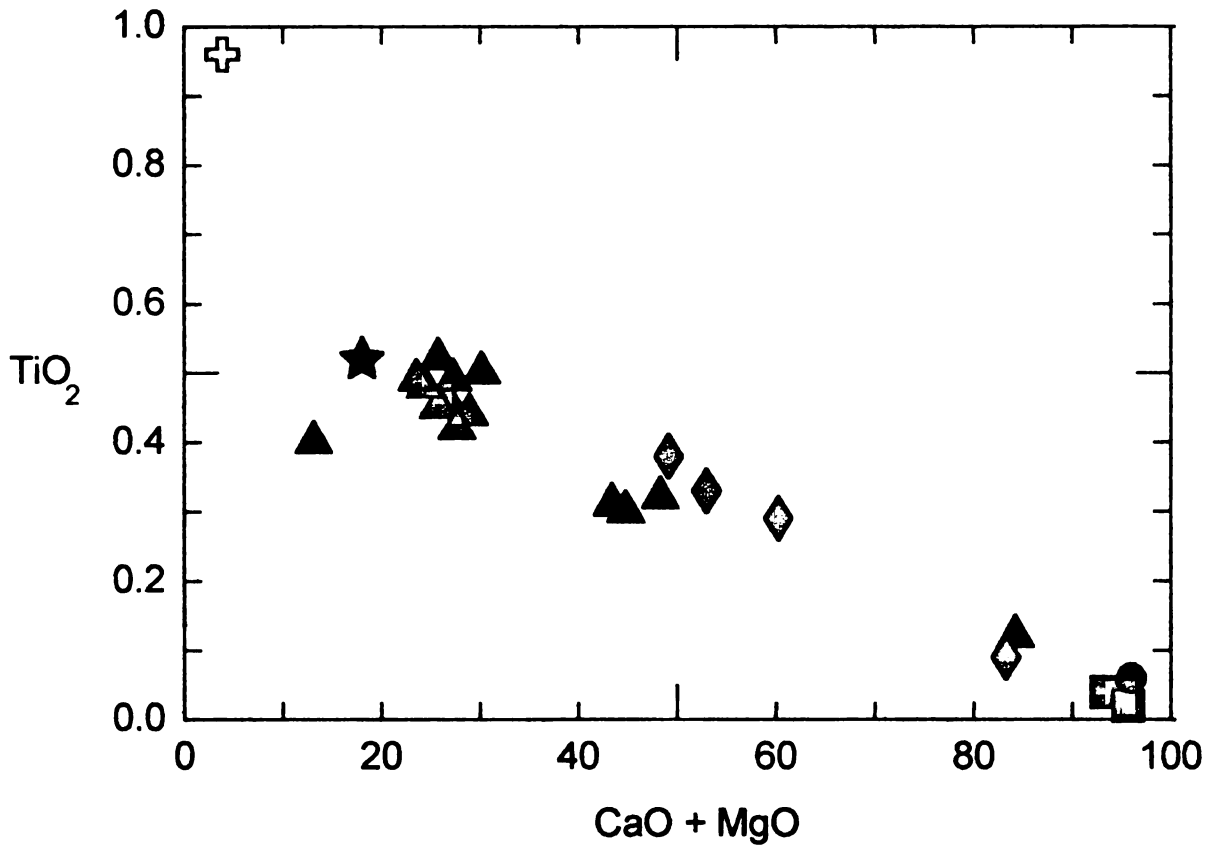

Figure 13. Plot of XRF data showing trend of decreasing TiO_2 with increasing CaO + MgO. Triangles = U5 samples; diamonds = U7 samples, squares = U6 samples; cross = Y6 sample; star = Y4 sample and circle = Y1 sample.

Figure 14a-b. a) Plot of XRF data showing the trend of increasing Zr with increasing SiO_2. Triangles = U5 samples; diamonds = U7 ; squares = U6 samples; cross = Y6 sample; star = Y4 sample and circle = Y1 sample; b) Variation of Zr with depth in the U5 well.

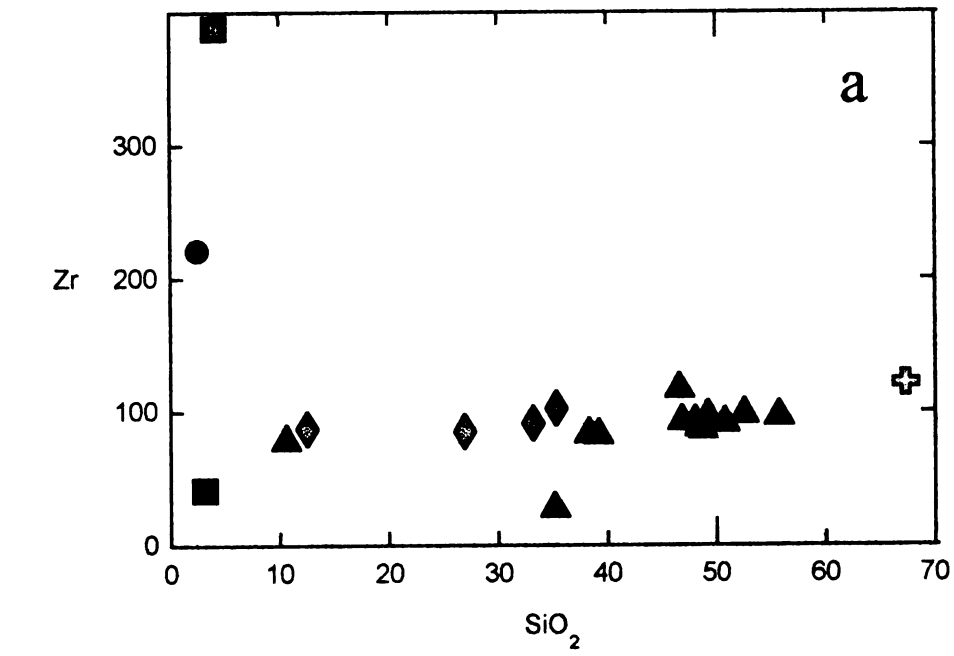
a
300
200
100
0
Zr
0
10
20
30
40
50
60
70
SiO2

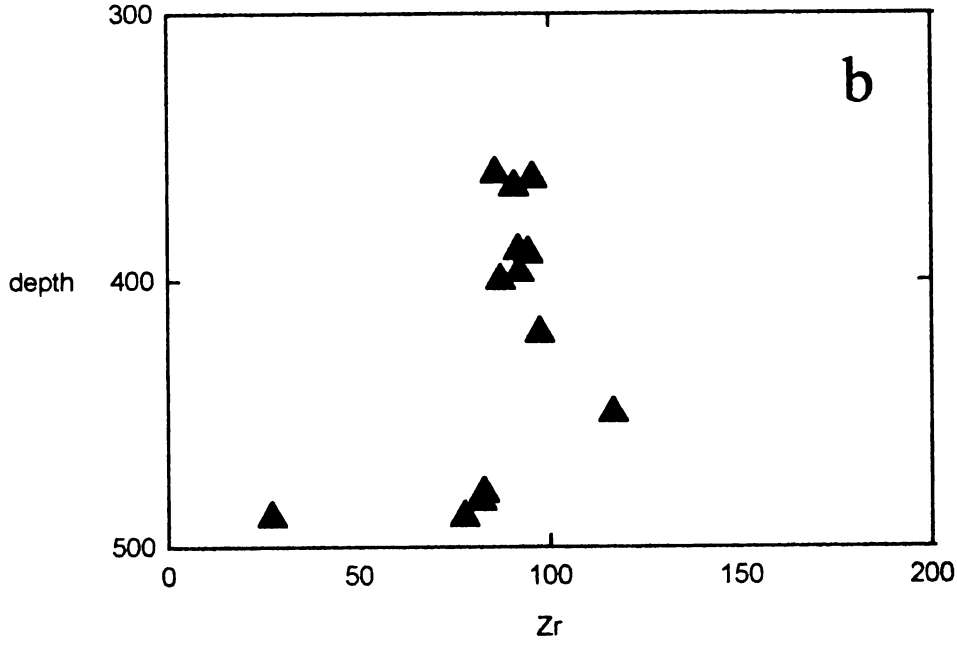
b
300
400
500
depth
0
50
100
150
200
Zr

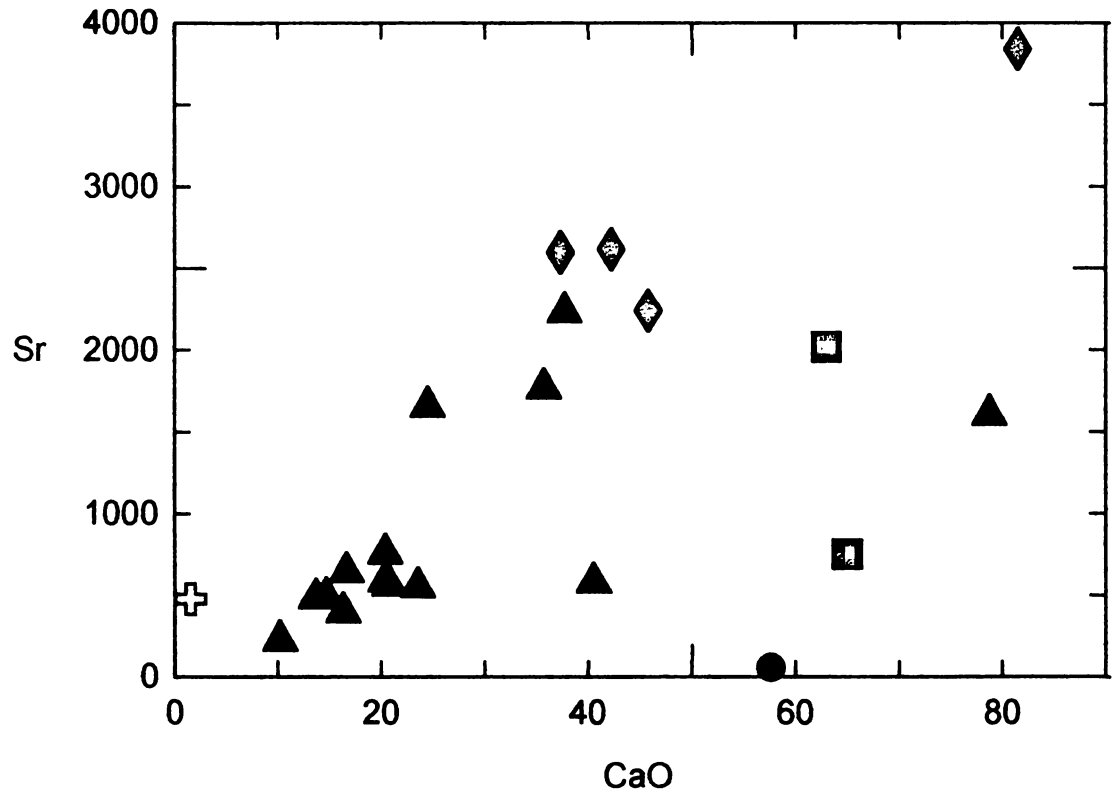

Figure 15. Plot of XRF data showing trend of increasing Sr with increasing CaO. Triangles = U5 samples; diamonds = U7 samples, squares = U6 samples; cross = Y6 sample; star = Y4 sample and circle = Y1 sample.

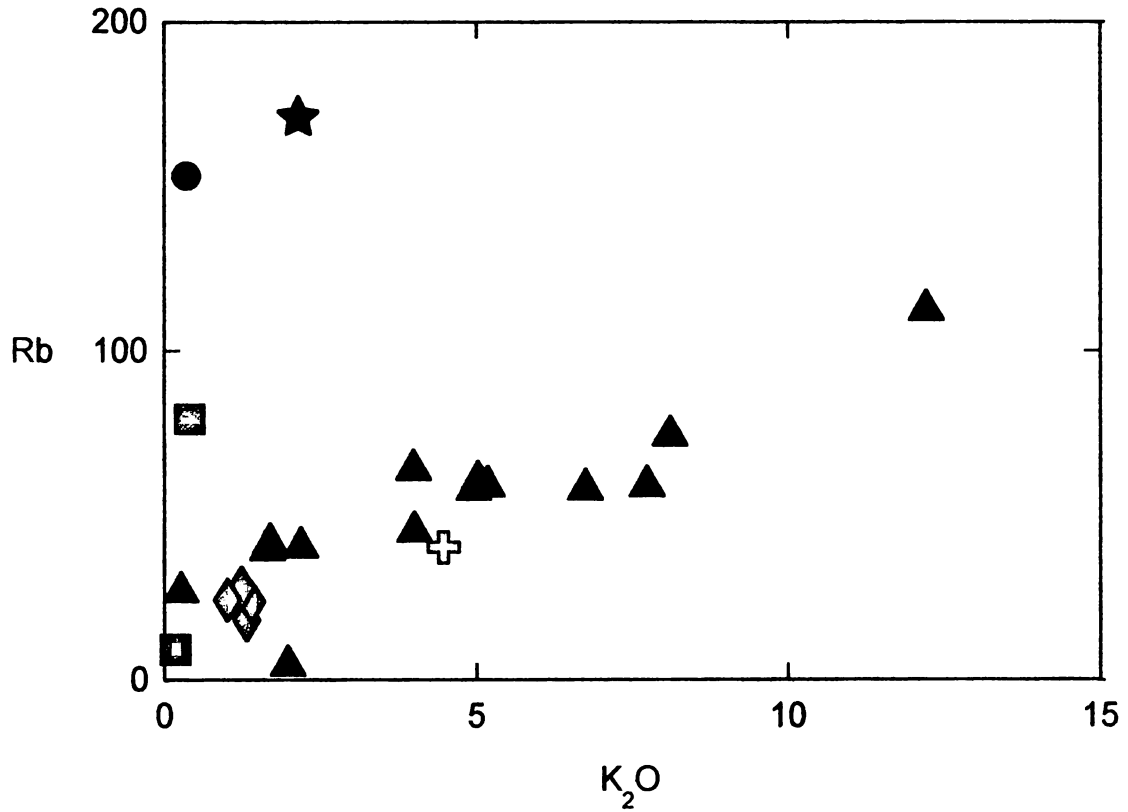

Figure 16. Plot of XRF data showing trend of increasing Rb with increasing K_2O. Triangles = U5 samples; diamonds = U7 samples, squares = U6 samples; cross = Y6 sample; star = Y4 sample and circle = Y1 sample.

an increase in CaO (Figure 15). Rubidium shows an increase in abundance with increasing K_2O (Figure 16).

Electron Microprobe Results

The results from the Electron Microprobe studies show changes in matrix compositions over very small scales. Elemental maps of two areas on the thin section U5-420-b can be seen in Appendix D. The first of six sections in each set (2 images) is a back-scattered image of the region of interest. Each section thereafter is labeled at the bottom. Scales are included for both length and counts (colored scale, in units of counts).

Each image was taken from a region within the thin section that represented a transition from one type of breccia to the other. Figures 48 and 49 represent a region in the upper boundary region of Figure 43, while Figures 50 and 51 represent a more centrally located boundary region. Within these elemental maps, small scale variations in the matrix materials can be seen. The elemental maps most useful for distinguishing these small scale variations are those for Si, Al, Mg and Ca, which exemplify the components most prominent in the two types of breccia present in the samples and the transitions between them. Elemental maps for sulfur are also helpful in determining the presence of sulfate minerals.

Textures and Petrology of Chicxulub Impact Breccias

In examining the breccias from the Chicxulub crater both in hand sample and in thin section, it is immediately apparent that the two types of breccia (suevite and Bunte-type) have distinctly different textures. The matrix of these breccias generally consists of pieces of brecciated rocks within a very fine grained groundmass, thus, they are termed polymict breccias. Fragments range in size, in the selected samples, from 1 mm to 1 cm. Fragments smaller than 1 mm are plentiful, but are considered part of the groundmass. In this study, clasts are defined as grains over 1 mm in diameter (in at least one dimension).

Samples from the U5 and upper portions of the U7 wells contain much more melt rock than do those from the lower portions of U7 and the U6 wells. They tend to have a darker colored matrix, as well. The processes of identifying clast types and distinguishing matrix from clastic material is markedly easier in the Bunte-type breccias, as the overall samples become much less altered. In all of the samples examined, however, clasts occur that are the same color/rock type as the matrix itself. This is especially true in the U7 and U6 wells. It becomes difficult, in this case, to decide whether to classify such features as clasts or matrix.

Hand sample analyses

The breccias from the Chicxulub impact are extremely complicated in their nature. This is readily apparent when one begins to look at hand samples of these rocks. Many variations exist within and among the hand samples from the three UNAM wells. Detailed descriptions and photographs of representative hand samples of each breccia type can be found in Appendix A. General observations from each well are as follows.

Within the U5 well, the number of silicate clasts decreases with depth. The abundance of reaction rims around clasts also tends to decrease with depth. In this well, large fragments tend to be more angular than smaller fragments (2 mm and less), and the smaller fragments tend to become more angular with depth. The existence of cavities within the matrix (from plucked grains) and within clasts themselves tends to increase near the middle of the sampled section of the well, (depths in the high 300 m area), and tends to decrease sharply after approximately 415 m depth. This defines a range of approximately 40-50 m with a large number of cavities. The fine grained matrix material in the well is greenish in color near the top, tan-gray in color in the middle, and a darker brown near the bottom. The abundance of light colored (carbonate and evaporite) clasts tends to increase toward the bottom of the well. Breccias-within-breccias are apparent throughout samples from this well.

The trends in the U5 breccias seen in this study are compatible with those seen by Sharpton et al., (unpublished), who have divided the U5 well into

subunits, based on changes in the character of the core samples. These subunits are shown in Figure 17.

Within the U7 well, some major differences exist. Samples from the shallower portion of this well are similar in appearance to samples in the U5 well. They are tan/gray in matrix color, and, though some darker clasts exist, light colored clasts are most prevalent. The matrix is more fine grained in these samples, lacking many of the sub-millimeter sized fragments found in the U5 samples. Clasts seem to be of a smaller size, in general, near the bottom of the well, though the clasts tend to be more angular in all of the U7 samples relative to the U5 wells as a whole. No cavities exist in these samples and reaction rims are rare. Breccias-within-breccias do occur in this well.

The U6 well appears to be fairly uniformly composed of a very fine grained light tan colored matrix. Very few sub-millimeter sized grains exist as part of the matrix. The small clasts that do exist tend to be very angular. Most clasts are light colored though some darker clasts do exist.

The Yucatan-6 samples contain large, angular mostly dark, gray and green clasts. The clasts are numerous and this rock type would be considered clast supported. Very few cavities exist. Clasts here tend to contain pre-impact igneous and metamorphic textures.

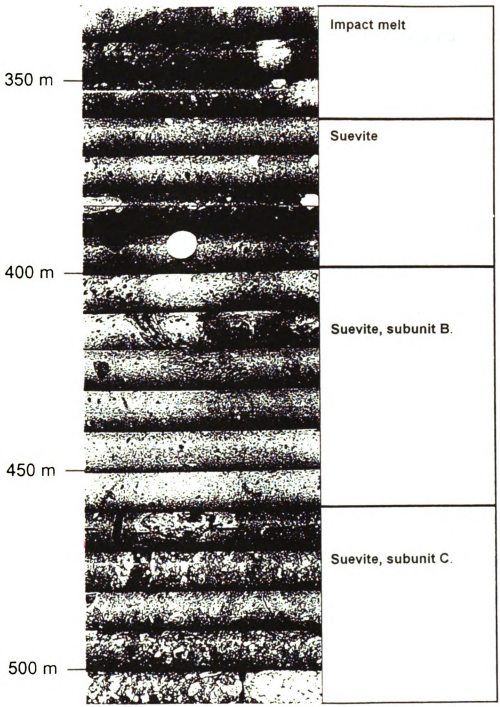

Figure 17. Images of drill cores from the U5 well and the subunits designated by Sharpton et al. (unpublished).

Petrography

Many thin sections from the Chicxulub impact rocks were examined briefly. Point counting was conducted from nine thin section images in an attempt to quantify the abundances of different minerals and textures occurring in these breccias. Details of this procedure can be found on pages eight and nine. Results can be seen in Table 5.

In studying these thin sections, it is apparent that much of the mineralogy is remnant from the pre-impact stratigraphy discussed on page six. Many textures from the pre-impact lithologies are still visible within these rocks, though many new and unusual textures have formed.

Mineralogy

The major minerals in existence in the Chicxulub cores include quartz, calcite, dolomite, anhydrite, gypsum and halite. These minerals appear not only as individual crystals and grains, but are the major components of the matrix. Minor minerals must have included such minerals as K-feldspar, hornblende and biotite. Garnets have also been identified within individual basement gneiss clasts (Sharpton et al., unpublished). In many cases, melt rocks have been subsequently altered to clay minerals, most frequently chlorite.

In examining the breccias, particularly in thin section, it is apparent that the mineralogy changes drastically between the two breccia types. In the Bunte-type breccias, the matrix becomes much easier to distinguish from the

clasts, and individual crystals become much easier to identify compared to the suevitic breccias. In the Bunte-type breccias, evaporites become more prevalent, as much more anhydrite appears as clasts and individual grains, and gypsum also appears as clasts, grains and veins.

Textures

In examining the impact breccias under the microscope, it is apparent that they are even more complicated than they appear in hand sample. Many complex but fascinating textures appear within these sections, each containing a wealth of information. Some of the most important and frequently recurring textures of these sections are discussed below. Their significance will be discussed later. Images of all thin sections examined appear in Appendix C.

The suevitic breccias, found throughout the entire U5 well and portions (possibly only upper portions) of the U7 well, contains many distinct textures. These include many associated with the matrix, the melting and mixing of target rocks and the subsequent alteration of these melts to clay minerals. Others include clasts that may not have not been altered whatsoever. Matrix textures are generally fine grained matrix (Figures 18, 19), where grains are so small or so shocked/melted that they are indistinguishable. These matrices can appear homogeneous, as in Figure 18, or very heterogeneous, as in Figure 18. Some instances show more than one type of matrix in each thin section (Figure 19), where areas of completely different mineralogy lie

Figure 18. Image of U5-450-b, a suevitic breccia, showing heterogeneous fine grained matrix of suevites, anhydrite clasts and crystals, rimmed clasts and clasts altered to clay minerals. Image was taken from thin section under crossed polars at 2.5x power. Field of view = 3.5 x 2.5 mm.

Figure 19. Image of U5-450-b, a suevitic breccia, showing heterogeneous matrix, shocked quartz with planar deformation features, rimmed clasts, and clasts altered to clay minerals. Image was taken from thin section under uncrossed polars at 2.5x power. Field of view = 3.5 x 2.5 mm.

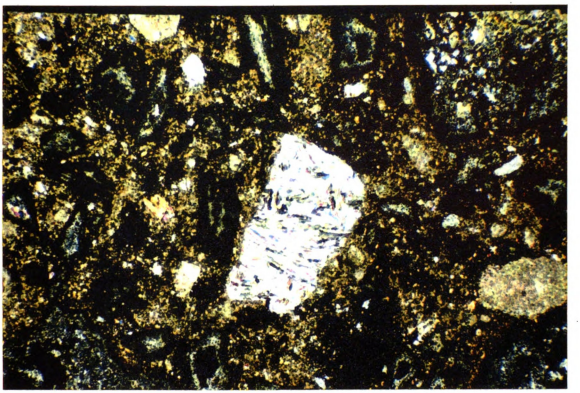

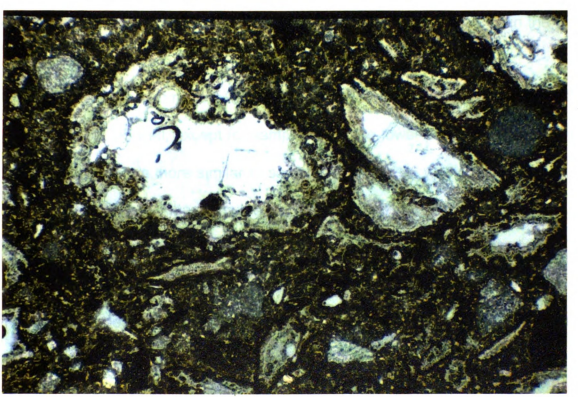

intermingled with the matrix that makes up the majority. Rimmed clasts occur frequently in the upper portions of the U5 suevites (Figure 18, 19, 20) where temperatures of clasts were different than that of the matrix during formation. Areas around clasts also appear to have reaction characteristics, though not necessarily in coherent rims (Figure 20). Breccias-within-breccias occur somewhat frequently, usually appearing as an irregularly shaped clast containing clasts within its boundaries (Figure 21). Highly shocked and melted materials may result in such things as impact glasses (Figures 19, 20, 21), vesicular melt clasts (Figure 21) and melt clasts that appear to have flow structures within them (Figures 20, 21). Figure 19 shows a typical carbonate clast in a suevitic breccia, while Figure 18 shows a typical anhydrite clast in a suevitic breccia. Many clasts have been altered to clay minerals. A few of these examples occur in Figure 18, 19. Figure 41 (U5-383-2a) and Figure 43 (U5-420-b) in Appendix C show the two large silicate clasts that appeared in the thin sections examined.

The samples from the lower U7 well tend to be similar in texture types to those from the U5 well, except for samples from the lower portions of the boundary, which are more similar to samples from the U6 well (Sharpton et al., unpublished). These latter samples are of the Bunte-type. There are a few textures of these breccias worth noting. The matrix of the thin sections from U7 seem to be made up of less shocked and altered material than those in U5. The matrix appears to be more consolidated and homogeneous, and contains fewer sub-millimeter fragments. Examples of this matrix can be seen in

Figure 20. Image of U5-450-b, a suevitic breccia, showing a large , rimmed, melt clast exhibiting flow structures. Other rimmed clasts are also seen. Image was taken from thin section under uncrossed polars at 2.5x power. Field of view = 3.5 x 2.5 mm.

Figure 21. Image of U5-450-b, a suevitic breccia, showing a larger melt clast exhibiting flow textures. Image was taken from thin section under crossed polars at 2.5x power. Field of view = 3.5 x 2.5 mm.

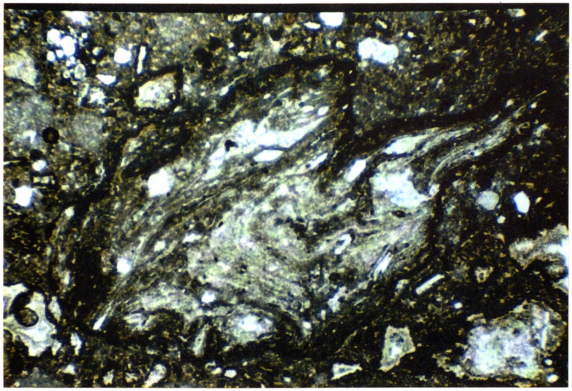

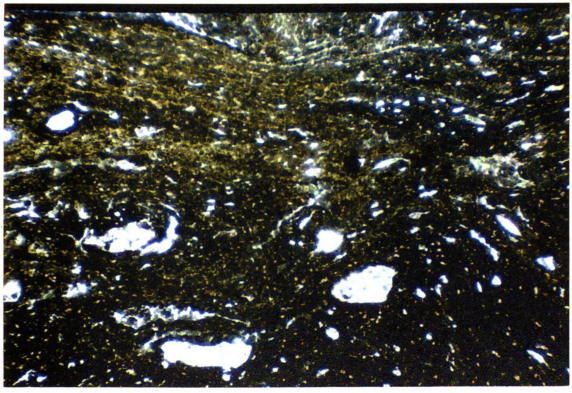

Figure 22. Image of U7-658-b, a Bunte-type breccia, showing different types of matrix, fossils, anhydrite crystals, and clasts altered to clay minerals. Image was taken from thin section under crossed polars at 2.5x power. Field of view = 3.5 x 2.5 mm.

Figure 23. Image of U7-658-b, a Bunte-type breccia, showing different types of matrix, anhydrite clasts, individual anhydrite crystals, and clasts altered to clay minerals. Image was taken from thin section under crossed polars at 2.5x power. Field of view = 3.5 x 2.5 mm.

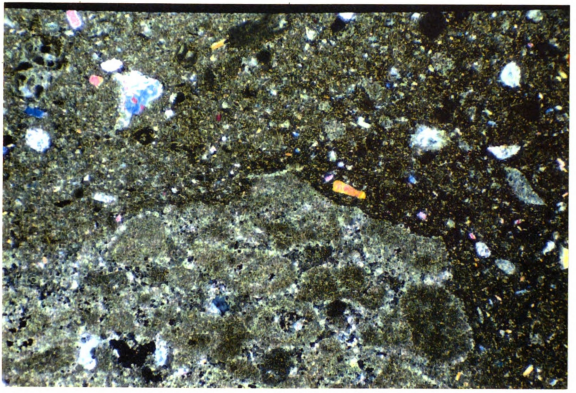

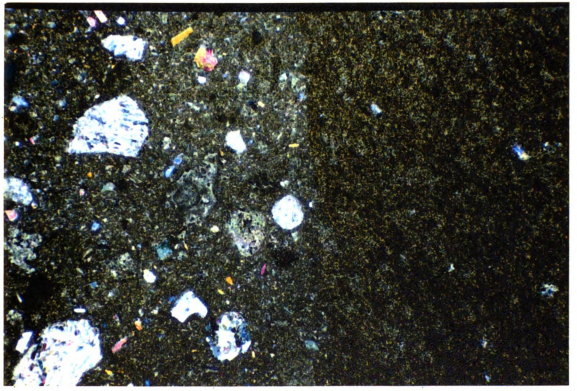

Figure 24. Image of U7-658-b, a Bunte-type breccia, showing fossils and typical clasts, including anhydrite and calcite. Image was taken from thin section under crossed polars at 2.5x power. Field of view = 3.5 x 2.5 mm.

Figure 25. Image of U7-658-b, a Bunte-type breccia, showing homogeneous matrix next to a large anhydrite clast, which exhibits large, individual, bladed crystals. Image was taken from thin section under crossed polars at 2.5x power. Field of view = 3.5 x 2.5 m m.

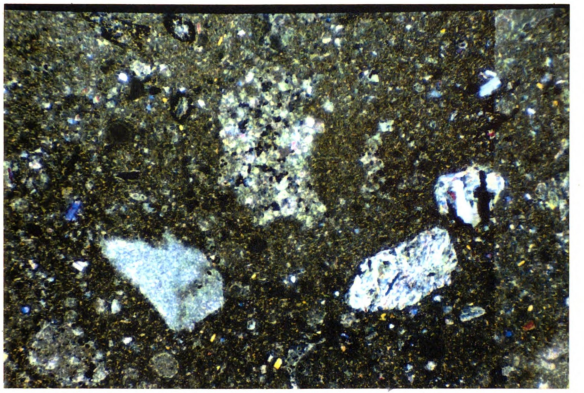

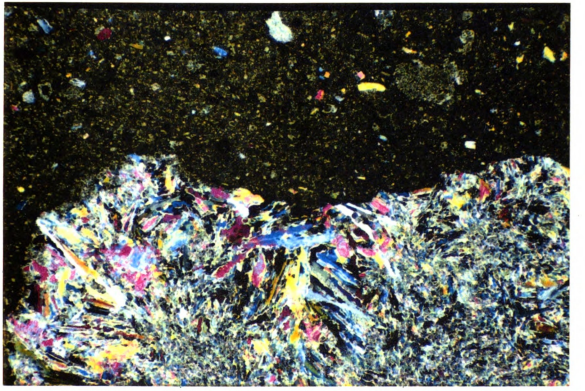

Figure 26. Image of U7-658-b, a Bunte-type breccia, showing separate foraminifera fossils as well as a fossiliferous matrix. Anhydrite clasts and crystals also exist. Image was taken from thin section under crossed polars at 6.5x power. Field of view = 1.5 x 1.0 mm.

Figure 27. Image of U7-658-b, a Bunte-type breccia, showing foraminifera fossils, anhydrite clasts and crystals, a silicate clast and clasts altered to clay minerals. Image was taken from thin section under crossed polars at 2.5x power. Field of view = 3.5 x 2.5 mm.

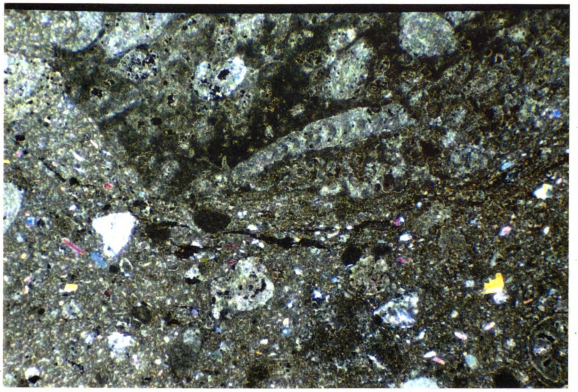

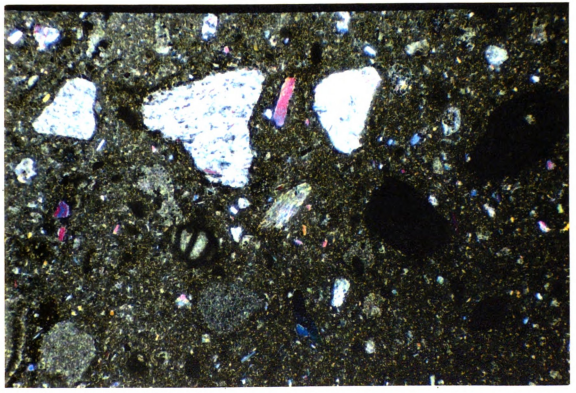

Figures 22-27. Different types of matrix do occur simultaneously in these samples, also, as shown in Figures 22 and 23. Anhydrite occurs more frequently in the U7 section, examples of which are shown in Figures 23, 24, 25 and 27. Anhydrite crystals tend to be larger in these samples than they were in the U5 samples. Anhydrite crystals also occur as individual grains within the matrix, as seen in Figures 23, 24, 25, and 27. Silicate clasts occur U7 samples, as well, shown here in Figure 27. One of the most important differences in the thin sections of the Bunte-type breccias as opposed to those of the suevitic breccias lies in the fact that fossil fragments appear in the Bunte-type breccias. These fossils (Figures 24, 26, 27) are most likely benthic foraminifera (Anstey, R., personal communication, and Sibley, D., personal communication) and are similar to those shown from K/T sites in Belize by Ocampo et al. (1996) (Figure 28). Gypsum also occurs in these breccias, particularly as veins, as portrayed in Figure 46.

Interpretation and Discussion

Textural variations within drill core samples

Textural trends with increasing depth in the U5 crater suggest that the materials in this well are allogenic (i.e., have not been transported far from their source location) and have been exposed to conditions harsh enough to cause their melting, shock and thermal alteration. They also imply that the thermal

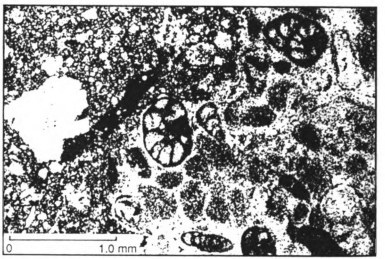

Figure 28. Similar fossils found in K/T impact deposits from Belize (from Ocampo et al., 1996).

regime within the well decreased towards cooler, less shocked materials with depth.

Textures such as the angularity of clasts can indicate the amount of alteration a clast has seen since it was broken from its source rock. Just like a grain in a sedimentary environment, the more rounded the clast, the more action it has seen. Angularity of breccia clasts seems to decrease with the intensity of thermal alteration and shock.

Reaction rims around clasts indicate that the temperatures differences existed between the clasts and matrix. These differences were enough to cause a chemical reaction to occur where the two materials met. This is the result of the fact that heat will flow towards colder materials and could have been either cold clasts falling into hot matrix, hot clasts falling into cooler matrix. The fact that these rims are most prevalent in the middle portion of the U5 well indicate that conditions here were a combination of the upper well (too hot for rims to form - everything was melted) and lower well (temperatures were too cool for reactions to occur) temperature regimes.

Cavities in the U5 well are also indicative of extreme thermal conditions. These cavities are either a result of melt clasts being dissolved post impact, plucked during sampling or are vesicles containing trapped gases which formed during impact. These cavities occur most frequently in breccias from the intermediate depths of the well containing less overall melt and a more siliceous matrix.

The matrix variations within the U5 well hold important implications in themselves. The fact that the amount of melt in the breccias (clasts and matrix combined) varies from high in the upper portions of the well (to about 400 m depth) to lower in the intermediate portions of the well (400 to ~460 m depth) and then again to high amounts of melt in matrix in the lower portions of the well (> ~460 m depth) suggest a layering of types of emplacement of target materials within the topographic basin itself. This layering could be the result of the emplacement of minor amounts of carbonates mixing with the first-encountered highly melted basement rocks, followed by the next layer of basement rocks which were thrown into the air on impact and later redeposited on top of the initially melted materials, allowing them to have experienced lower temperatures. On landing, then, these materials were re-exposed to high temperatures, causing the formation of reaction rims. Deposited on top of these breccias were the most highly shocked and melted materials from the deepest depths of excavation, which were thrown into the air after the earlier deposited rocks, or may have moved over them in a fluid type manner, as indicated by flow textures within these deposits. The final layer to have been deposited in the U5 well was the fluidized impact melt sheet, in which almost every particle has either been highly altered or melted completely, and the matrix is made up of almost entirely melt.

Breccias found within other breccias (i.e., breccias making up clasts themselves) are probably formed during the above processes. As one type of material is broken up (brecciated) and thrown into the air, it can easily be

caught up in the deposits from the next set of materials to be ejected, as speeds of ascent and descent probably vary among the different materials.

Samples from the lower portion of U7 and from all of the U6 well exhibit textures drastically different from those of the U5 and upper U7 wells. Fossil fragments exist, indicating that these rocks could not have been exposed to a large degree of shock. If they were exposed to a large degree of shock, the fossil fragments would have been destroyed instead of just replaced. Large veins of evaporites, especially in the U6 well, where the upper portions of the breccias are riddled with gypsum veins (Sharpton et al., unpublished). The limited occurrence of silicate materials in these breccias indicates that silicate materials (lower target) were not ejected as far out as carbonate and evaporitic materials (upper target).

Textural trends moving away from the center of the crater include, generally, decrease in the number of clasts, decrease in highly shocked and melted materials including basement clasts and glass, and decrease in features such as cavities, reaction rims, breccias within breccias and increased angularity in clasts. These trends reinforce the conclusions from the chemical data (discussed below) that upper target materials were transported farther from ground zero than were those from lower target locations. They also indicate that materials from the upper target were less shocked, less melted and less thermally metamorphosed than were those from the lower target. High degrees of shock and thermal alteration are indicated by features discussed above, such as cavities, reaction rims, less clast angularity, flow

features in melted clasts, etc. Lack of these features in distal deposits suggests that they have not been subjected to such conditions.

Chemical variations within drill core samples

There are a number of chemical trends in the major and trace element data (determined from XRF analyses) from the Chicxulub impact breccias. These trends include the decrease in SiO_2 and Al_2O_3 and increase in CaO and MgO with distance from the center of the crater. As the target stratigraphy is composed of carbonates and evaporites overlying a silicate basement, one interpretation is that the silicate materials were thrown higher (or at a steeper angle) into the air upon impact than the carbonate platform rocks, causing them to land after, and, thus, on top of, the carbonate materials. Carbonate materials were thrown out at a shallower angle and were thus ultimately located farther out from the crater's center. This is in addition to the simpler interpretation that, since the silicate materials were thrown out just an instant after the carbonate materials, they would have landed on top of them.

The U5 well did not intercept the bottom of the suevite unit during drilling. It is assumed that there is a significant amount of this breccia below the core bottom, and it is possible that it becomes even more carbonate rich. Whether or not the boundary between the suevitic breccias and the Bunte-type breccias would be found deeper in the well is unknown, but it is a possibility.

Within the U5 well, there also exists a trend of decreasing SiO_2 and Al_2O_3 and increasing CaO and MgO with increasing well depth. This trend reflects

the same process stated above - the deeper target (i.e., silicate material) lands after the shallower target (carbonate materials). There would inevitably be some mixing of the two during this event, resulting in the gradual increase in carbonate with depth as is shown in the Chicxulub breccias in U5. This increase in carbonate can be seen somewhat in the slight increase in clasts of limestone and dolomites, but is likely to be more associated with increasing portions of fine grained carbonates in the matrix material.

The increase in carbonate material with depth in the U7 well, and especially the marked contrast in SiO_2 and CaO values between the upper and lower samples, indicates that there exists a boundary between the suevites and Bunte-type breccias (Corrigan et al., 1997). The nature of this boundary is not evident from these data, but data from Sharpton et al. (unpublished) indicate that it is very sharp.

Trends of high K_2O abundances in rocks from the upper sections of U5 would be expected if the material being melted contained minerals such as K-feldspar. The most K_2O exists where the most basement material was deposited. As the basement rocks in the Chicxulub target were generally gneissic, this is an expected result.

Trends of high Na_2O abundances would also be expected in rocks from the upper sections of U5, as minerals such as plagioclase feldspars, containing a significant amount of sodium, would be prevalent in the silicate basement rocks.

Trends of high Fe and TiO_2 abundances would also be expected in rocks from the upper sections of U5, as they are typically found in ilmenite, ($FeTiO_3$), a mineral common in silicate basement rocks. Thus, the trends of increasing TiO_2 with increasing SiO_2 and decreasing TiO_2 with increasing CaO+MgO (Figure 13) would be expected.

The MgO trends seen in the Chicxulub rocks may be the result of two competing scenarios. MgO values tend to be somewhat increased in the mafic minerals basement rocks. MgO is also high in the sedimentary mineral, dolomite, which seems to be a large component of the Chicxulub target stratigraphy. The result, as shown in Figures 7, 9, and 11-a, shows two distinct trends in MgO. One for the suevitic breccias, where MgO gradually increases as CaO+MgO increases, and one where MgO increases very sharply as CaO+MgO increases. This is a further implication that there is a large distinction between the chemical makeup of the two breccia types, and the distinct break in the trends is another indication of the boundary between the two breccia types within the U7 well (note U7 samples in Figures 7, 9, 11-a).

Trace element trends were somewhat expected, as well. As the trace element zirconium is the major constituent of the mineral zircon which has been found in many K/T deposits (Sharpton et al., 1996) associated with basement rich breccias. It is not unexpected, then, that plots of Zr vs. SiO_2 show a trend of increasing Zr with SiO_2. Strontium increasing with increasing CaO is also an expected trend. Strontium tends to be an important trace element abundant in carbonate minerals. The same is true for barium, which

also shows a general increase with increasing CaO. Rubidium showing a positive correlation with K_2O is also to be expected, as it is an incompatible element and would be the first to be transported into the materials melted upon impact. Here the silicate breccias are rich in K_2O, as exemplified earlier, which would also cause them to be rich in Sr.

The results of Electron Microprobe elemental mapping analyses (Appendix D), which show small-scale variations in the matrix compositions are expected. During the emplacement and resultant combining of the many different components present in the target material, interactions between possibly fluidized portions would be expected.

Probably the most important implication of these chemical data, however, is the abundance of SiO_2 in the U5 and U7 wells. Prior to the onset of this study, silica-rich breccias (i.e., suevitic breccias) were not thought to occur as far out as the U5 well, let alone as far out as the U7 well. The fact that a layer of melt rock also exists above the suevites in U5 is even more unexpected. Prior studies (Sharpton et al., 1996) show melt and melt breccia rocks occurring below suevitic breccias in wells C1, S1 and Y6 (approximately 25, 30 and 45 km from the center of the crater, respectively). No suevitic breccias appear in the stratigraphy of the Ticul 1 well at all (~95 km from crater center). The results presented here, which indicate the presence of suevitic breccias in both wells U5 and U7 (110 and 125 km from crater center, respectively) and melt rock occurring on top of U5 suevites is an important discovery. The importance of this finding lies partially in the debate over the

size of the Chicxulub impact crater. If the suevitic breccias are allogenic, or crater-fill breccias (Sharpton et al., 1996) (those deposited in place, or here, within the initial crater rim), then their presence at a distance of 125 km (the U7 well) might indicate something about the initial size of the crater's topographic basin rim. To accommodate these materials as far out as 125 km, the initial diameter of this rim would have had to have been at least 250 km. Since the suevite breccias do not exist in the U6 well (or if they did they have eroded away), which lies at ~150 km from the crater's center, we can put a bounding limit on the crater's maximum size of 300 km. This creates, then, a range for the initial size of the Chicxulub crater from 250 km to 300 km in diameter. These interpretations, however, are only applicable for the south, or landward, side of the crater, as these are the only deposits which have been sampled to date. Whether these same characteristics hold true for the rest of the crater, i.e., whether the crater is symmetrical, remains to be seen.

Conclusions

Studying the breccias from drill cores of the Chicxulub impact crater have given us new insights into the way ejecta is distributed around a crater and into the Chicxulub event and the characteristics of the resulting crater. This study gave an unprecedented look at the breccias formed by this impact and have reshaped some of the ideas about where certain types of materials now reside and what this may imply.

The U5 well, in particular, has given a wealth of new insight into the crater's structure and formation. The variations with depth within this well alone indicate a complex thermal regime, with temperatures and degree of shock decreasing with depth. The materials in this well range from impact melt to melt-clast rich breccias to breccias with less overall melt and finally to breccias with a melt-rich matrix. This implies that materials from different depths in the target rocks end up stacked in an inverted manner, as is evident in the Ries crater. This evidence is supported even further by comparing the chemical compositions of breccias from the U5 well to those in the U6 well. The drastic difference in chemical make-up between the two indicates that the U5, or suevitic breccias, are derived from rocks at depth (silicate basement) and those in U6, or Bunte-type breccias, are derived from rocks at shallow depths in the target stratigraphy (carbonates and evaporites). The breccias from the U7 well indicate that a boundary exists between the two types of breccia, with suevitic breccias lying on top of Bunte-type breccias. The nature of this break (whether it is sharp or graded), however, can not be accurately determined from these data. The nature of this boundary is an important topic, as it holds many implications as to the type of mechanism responsible for emplacement of the two types of breccia (whether it be ballistic emplacement or more of a fluidized mass of material flowing over the Bunte-type breccias).

The fact that a large amount of silicate materials exist within the U5 and U7 wells indicates a large (250-300 km) initial topographic rim diameter for the

crater. This size is on the upper limit of diameters suggested so far by workers such as Sharpton et al. (1993, 1996) and Urrutia-Fucugauchi et al. (1996).

These and other new findings (Sharpton et al., unpublished) have increased the amount known about the rocks from the Chicxulub impact structure. Undoubtedly, these findings will serve as a basis for conducting more research into Chicxulub and other large impact craters in order to gain more insight as to how these impacts have affected the history of earth and the life it supports.

APPENDIX A

Figure 29. Photograph of the hand sample Y6-1196 (scale shown).

Figure 30. Photograph of the hand sample U5-338 (scale shown).

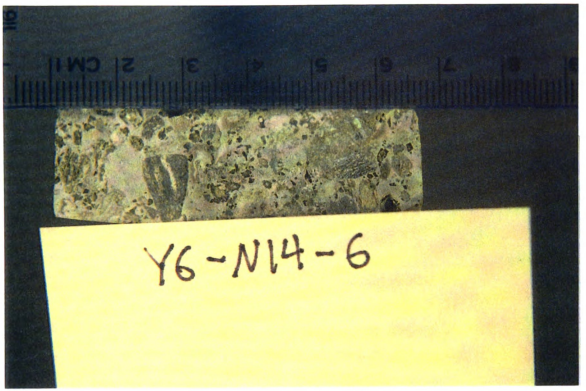
Y6-N14-6


U5-338-341

Figure 31. Photograph of the hand sample U5-360 (scale shown).

Figure 32. Photograph of the hand sample U5-390 (scale shown).

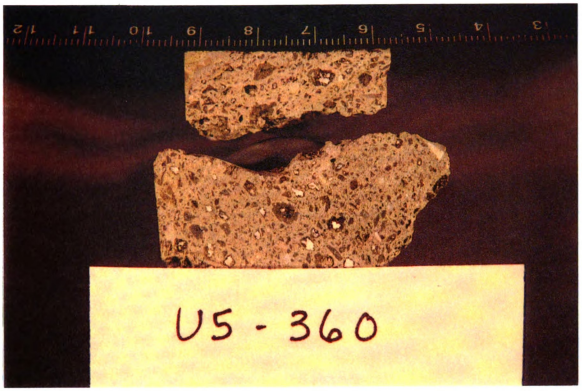
U5 - 360

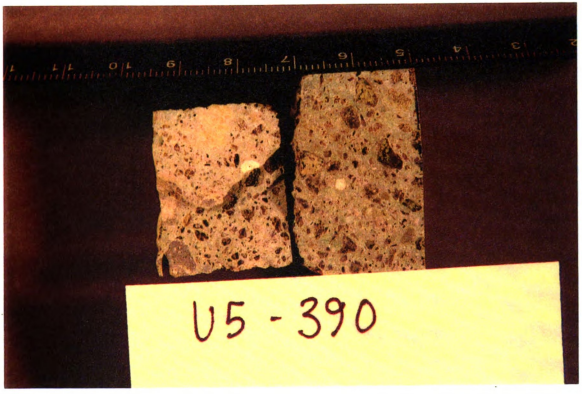
U5 - 390

Figure 33. Photograph of the hand sample U5-483 (scale shown).

Figure 34. Photograph of the hand sample U5-489 (scale shown).

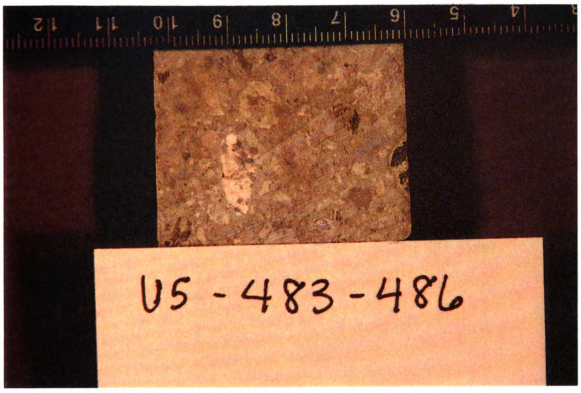
U5 - 483 - 486

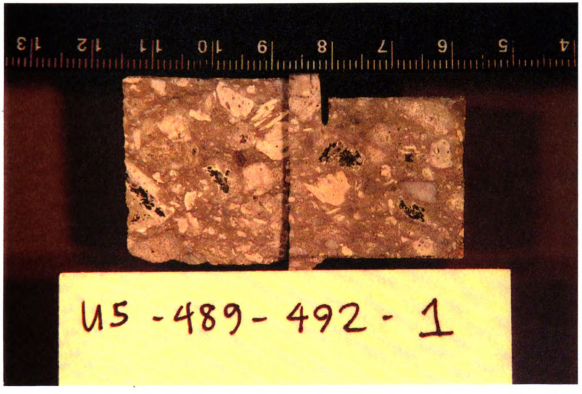
U5 - 489 - 492 - 1

Figure 35. Photograph of the hand sample U7-318 (scale shown).

Figure 36. Photograph of the hand sample U7-658 (scale shown).


U7 - 318

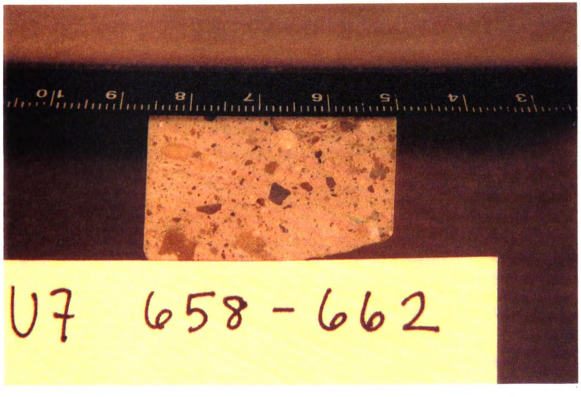
U7 658 - 662

Figure 37. Photograph of the hand sample U6-302 (scale shown).

Figure 38. Photograph of the hand sample U6-508 (scale shown).

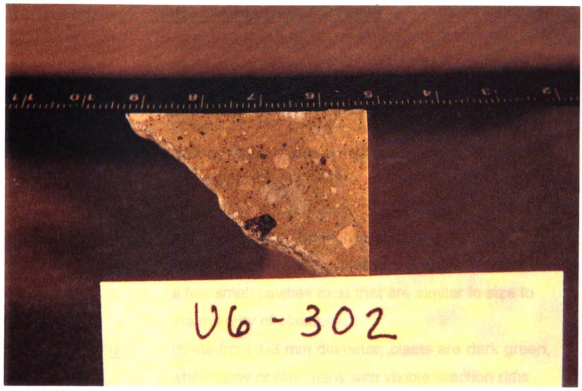
U6-302

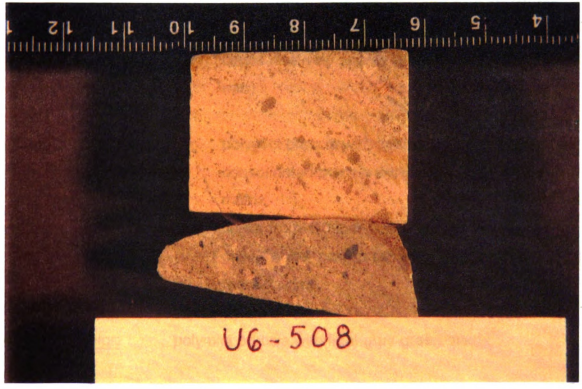
U6-508

HAND SAMPLE DESCRIPTIONS

UNAM 5:

U5-338m:
Color: green.
Texture: unconsolidated friable melt rock fragments.
Clasts: small clasts (< 2 x 2 mm).

U5-360m:
Color: polymict breccia with light gray-green matrix.
Texture: consolidated breccia with a very fine grained matrix; a few small cavities exist that are similar in size to the majority of clasts.
Clasts: clasts from 1-3 mm diameter; clasts are dark green, white, gray or tan, many with visible reaction rims.

U5-362m-1:
Color: polymict breccia with green matrix.
Texture: consolidated breccia with a very fine grained matrix with visible vesicles and flow structures (pores possibly somewhat oriented).
Clasts: clasts relatively sparse and small (< ~0.5 mm).

U5-362m-2:
Color: polymict breccia with light gray-green matrix.
Texture: consolidated breccia with a very fine grained matrix.
Clasts: clasts from 1-3 mm diameter; clasts are dark green, white, gray or tan, many with visible reaction rims.

U5-365m:
Color: polymict breccia with light gray-green matrix.

	Texture:	consolidated breccia with a very fine grained matrix; a few small cavities exist that are similar in size to the majority of clasts.
	Clasts:	clasts from 1-3 mm diameter; clasts are dark green, white, gray or tan, many with visible reaction rims.
U5-389m:	Color:	polymict breccia with light gray-green matrix.
	Texture:	consolidated breccia with a very fine grained matrix and numerous small, open cavities.
	Clasts:	clasts from 1-3 mm diameter; clasts are dark green, white, gray or tan, many with visible reaction rims.
U5-390m:	Color:	polymict breccia with light gray-green matrix.
	Texture:	consolidated breccia with a very fine grained matrix and numerous small, open cavities.
	Clasts:	clasts from 1-5 mm diameter; larger clasts here, which are cavities and/or exhibit reaction rims, though rimming appears to be decreasing.
U5-397m:	Color:	polymict breccia with light gray-green matrix.
	Texture:	consolidated breccia with a very fine grained matrix and numerous small, open cavities.
	Clasts:	clasts from 1-5 mm diameter; larger clasts here, which are cavities and/or exhibit reaction rims.
U5-400m:	Color:	polymict breccia with light gray-green matrix.
	Texture:	consolidated breccia with a very fine grained matrix and numerous small, open cavities.
	Clasts:	clasts from 1-5 mm diameter; larger clasts here, which are cavities and/or exhibit reaction rims; carbonate clasts are most frequently rimmed.

U5-412m:

Color: polymict breccia with light gray-green matrix.

Texture: consolidated breccia with a very fine grained matrix; fewer cavities exist here.

Clasts: clasts from 1-5 mm diameter; one large silicate basement clast exhibiting primary gneissic textures; less reaction rimming; one breccia-within-a-breccia.

U5-418m:

Color: polymict breccia with light gray-green matrix.

Texture: consolidated breccia with a very fine grained matrix; now with even fewer cavities than U5-412.

Clasts: clasts have decreased in size to 1-3 mm; little reaction rimming; clasts are lighter in color - mostly tan, gray and white.

U5-420m:

Color: polymict breccia with light gray-green matrix.

Texture: consolidated breccia with a very fine grained matrix and few cavities.

Clasts: clasts from to 1-3 mm; little reaction rimming; clasts are lighter in color - mostly tan, gray and white, though a few darker clasts do exist.

U5-450m:

Color: polymict breccia with matrix now more gray.

Texture: consolidated breccia with a very fine grained matrix and few cavities.

Clasts: clasts even smaller now, from 1-2 mm; rimming generally absent; still mostly light colored clasts with a few small darker clasts.

U5-480m: Color: polymict breccia with gray matrix.

Texture: consolidated breccia with a very fine grained matrix and few cavities; clasts seem to be arranged in a type of flow pattern.

Clasts: clasts small, from 1-2 mm; rims generally absent; mostly light colored clasts, with only one darker colored (green) clast.

U5-483m: Color: polymict breccia with gray matrix.

Texture: consolidated breccia with a very fine grained matrix.

Clasts: clasts small, from 1-2 mm; rims generally absent; mostly light colored clasts, with only one darker clast; a carbonate breccia-within-a-breccia exists in this sample.

U5-489m-1: Color: polymict breccia with very dark gray matrix.

Texture: consolidated breccia with very fine grained matrix; possible orientation of clasts.

Clasts: most clasts slightly larger - numerous 5 mm diameter clasts; most clasts are light colored (only ~25% darker clasts).

U5-489m-2: Color: dark gray.

Texture: fine crystalline.

Clasts: none - possibly a clast itself.

UNAM 6:

U6-302m: Color: polymict breccia with light tan matrix.

	Texture:	consolidated very fine grained breccia with 2 different matrices, one a bit darker tan than the other.
	Clasts:	clasts from 1-3 mm; fewer overall clasts and the vast majority are light colored (tan, gray and white) clasts.
U6-508m:	Color:	polymict breccia with tan matrix.
	Texture:	consolidated breccia, though coarser grained than other breccias.
	Clasts:	clasts 1-3 mm; far less clast abundance.

UNAM 7:

U7-244m:	Color:	polymict breccia with tan-gray matrix.
	Texture:	consolidated breccia with a very fine grained matrix.
	Clasts:	clasts generally 1-3 mm, though one large breccia-within-a-breccia exists; some clasts exhibit reaction rims; both dark (green, brown and black) and light colored (tan, gray and white) clasts exist.
U7-318m:	Color:	polymict breccia with gray matrix.
	Texture:	consolidated breccia with a very fine grained matrix.
	Clasts:	clasts from 1-5 mm now, most appear to be darker colored (many green clasts) and some melt.
U7-335m:	Color:	polymict breccia with gray matrix.
	Texture:	consolidated breccia with a very fine grained matrix.
	Clasts:	clasts 1-5 mm; 4-5 mm clasts exist all green; a breccia-within-a-breccia exists.
U7-699m:	Color:	alternating gray, tan and white.

Texture: very fine grained crystalline layers, possibly alternating silicate with carbonate.

Clasts: none; possibly a clast itself.

YUCATAN-1:

Y1-3151m: Color: gray.

Texture: fine grained uniform looking sample.

Clasts: none - possibly an anhydrite clast.

YUCATAN-2:

Y2-3330m: Color: tan and orange.

Texture: fine grained sandstone with some iron staining.

Clasts: none.

YUCATAN-6:

Y6-1196m: Color: polymict breccia with tan, gray and green matrix.

Texture: consolidated clast supported breccia with a very fine grained matrix that changes color between clasts; very few, if any, cavities.

Clasts: clasts vary in size from 1 mm to 1 cm and are very angular; most clasts are silicate and some exhibit primary igneous and metamorphic textures (though some carbonate clasts do exist); reaction rims exist on many clasts; many very opaque clasts exist (possibly sulfides).

APPENDIX B

Table 6: Whole rock XRF major element chemical analyses (normalized to 100%).

Sample	SiO_2	Al_2O_3	MnO	MgO	CaO	Na_2O	K_2O	P_2O_5	TiO_2	FeO
U5-360	48.75	10.77	0.10	10.35	16.36	1.36	7.74	0.11	0.46	5.29
U5-362-1	55.74	13.92	0.07	2.89	10.24	0.78	12.21	0.08	0.40	4.95
U5-362-2	49.22	11.08	0.09	9.11	16.65	1.33	8.11	0.12	0.45	5.07
U5-365	50.78	11.18	0.11	10.69	13.73	1.81	6.75	0.12	0.48	5.45
U5-389	48.04	11.35	0.07	6.92	20.41	2.91	5.03	0.12	0.49	6.32
U5-390	49.13	11.67	0.08	5.36	20.41	3.33	4.96	0.13	0.52	5.92
U5-397	46.87	11.50	0.08	5.37	23.57	2.84	5.18	0.12	0.44	5.50
U5-400	48.41	10.78	0.08	6.85	20.84	3.92	4.01	0.11	0.42	6.27
U5-420	52.55	11.51	0.10	8.85	14.72	3.49	3.99	0.12	0.49	5.10
U5-450	46.63	10.97	0.10	5.67	24.50	4.88	2.19	0.11	0.50	6.29
U5-480	38.32	8.35	0.07	7.08	37.73	3.47	1.70	0.05	0.30	5.49
U5-483	39.19	8.63	0.07	7.65	35.76	3.53	1.66	0.07	0.31	5.69
U5-489-1	35.17	8.25	0.08	7.75	40.54	2.66	1.98	0.07	0.32	7.11
U5-489-2	10.62	2.29	0.35	5.50	78.73	0.77	0.27	0.04	0.12	15.83
U6-302	4.14	0.79	0.00	28.42	65.00	0.87	0.41	0.02	0.04	1.22
U6-508	3.14	0.46	0.00	32.70	62.99	0.28	0.18	0.02	0.02	0.70
U7-244	26.92	6.47	0.08	14.43	45.80	1.98	1.32	0.08	0.29	6.11
U7-318	33.18	7.21	0.05	10.75	42.22	1.89	1.40	0.06	0.33	6.57
U7-335	35.28	8.05	0.03	11.79	37.34	2.22	1.24	0.06	0.38	7.81
U7-699	12.52	1.85	0.00	1.81	81.46	0.64	1.01	0.02	0.09	3.12

Table 6: (continued).

Sample	SiO_2	Al_2O_3	MnO	MgO	CaO	Na_2O	K_2O	P_2O_5	TiO_2	FeO
Y1-3151	2.46	0.65	0.00	38.33	57.62	0.21	0.35	0.02	0.06	0.31
Y4-N12	57.41	12.81	0.10	4.67	13.35	4.14	2.15	0.12	0.52	4.72
Y6-1196	67.35	13.69	0.09	2.29	1.58	3.58	4.47	0.25	0.96	5.74

Table 7: Whole rock XRF trace element chemical analyses.

Sample	Cr	Ni	Cu	Zn	Rb	Sr	Y	Zr	Nb	La	Ba
U5-360	n.d.	n.d.	n.d.	43.15	58.81	394.82	19.96	85.94	n.d.	n.d.	251.41
U5-362-1	n.d.	n.d.	n.d.	30.59	112.19	223.93	n.d.	95.61	n.d.	n.d.	280.92
U5-362-2	n.d.	n.d.	n.d.	49.21	74.13	640.34	14.99	95.71	n.d.	n.d.	422.01
U5-365	n.d.	n.d.	n.d.	50.59	57.88	482.42	20.21	90.84	n.d.	n.d.	384.76
U5-389-C	n.d.	n.d.	n.d.	48.89	60.26	754.56	19.35	91.88	n.d.	n.d.	382.92
U5-390	n.d.	n.d.	45.47	45.01	57.76	581.99	20.33	94.5	n.d.	n.d.	265.37
U5-397	n.d.	n.d.	n.d.	35.66	58.82	548.38	n.d.	92.19	n.d.	n.d.	164.94
U5-400	1205.95	140.01	n.d.	62.71	44.99	557.89	16.2	87.3	n.d.	n.d.	n.d.
U5-420	n.d.	n.d.	n.d.	44.75	63.75	491.24	19.29	97.47	n.d.	n.d.	369.32
U5-450	n.d.	n.d.	n.d.	31.53	40.2	1652	19.52	116.58	n.d.	n.d.	643.12
U5-480-C	n.d.	n.d.	n.d.	25.92	41.41	2227.97	n.d.	82.76	n.d.	n.d.	254.59
U5-483	n.d.	n.d.	n.d.	40.75	39.46	1764.22	n.d.	81.98	n.d.	n.d.	n.d.
U5-489-1	n.d.	n.d.	n.d.	27.69	n.d.	576.55	n.d.	27.26	n.d.	n.d.	n.d.
U5-489-2	n.d.	n.d.	n.d.	28.38	26.79	1601.93	n.d.	77.61	n.d.	n.d.	n.d.
U6-302-C	n.d.	n.d.	134.27	16.74	79.29	749.74	n.d.	387.72	n.d.	n.d.	n.d.
U6-508-C	n.d.	n.d.	n.d.	n.d.	n.d.	2017.32	n.d.	41.16	n.d.	n.d.	195.95
U7-244	n.d.	n.d.	n.d.	23.97	18.37	2240.54	n.d.	85.19	n.d.	n.d.	n.d.
U7-318-C	n.d.	n.d.	n.d.	27.93	23.81	2616.96	n.d.	91.26	n.d.	n.d.	n.d.
U7-335	130.93	n.d.	n.d.	42.07	27.97	2596.94	n.d.	101.99	n.d.	n.d.	129.48
U7-699-C	n.d.	n.d.	n.d.	n.d.	24.33	3841.19	n.d.	86.8	n.d.	n.d.	n.d.

Table 7: (continued).

Sample	Cr	Ni	Cu	Zn	Rb	Sr	Y	Zr	Nb	La	Ba
Y1-3151	n.d.	n.d.	n.d.	92.68	153.38	62.22	28.95	221.38	n.d.	n.d.	708.76
Y4-N12	n.d.	n.d.	258.12	33.35	171.08	5453.51	n.d.	706.62	n.d.	n.d.	n.d.
Y6-1196	n.d.	n.d.	n.d.	56.03	40.31	475.58	21.37	121.27	n.d.	n.d.	168.19

APPENDIX C

Figure 39. Thin section views (crossed and uncrossed polars) of the thin section U5-360-b. Field of view = ~ 40 x 25 mm.

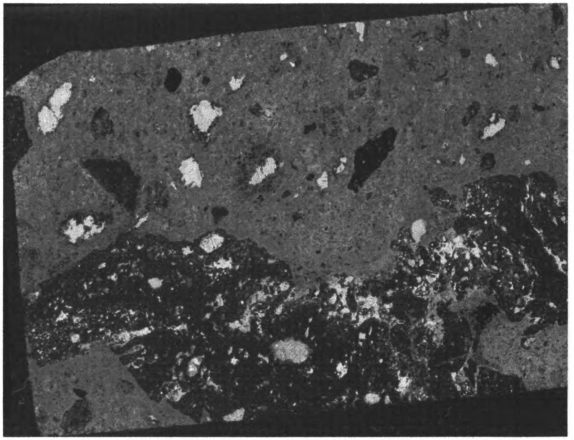

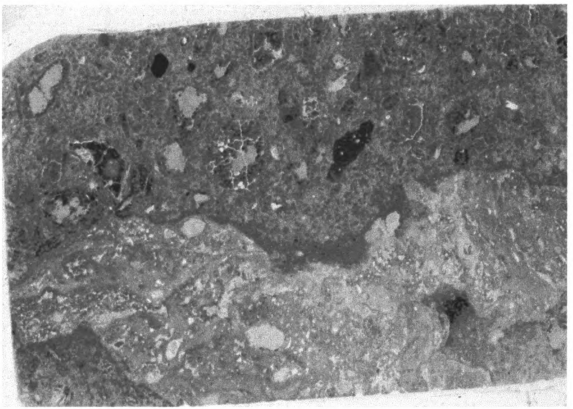

Figure 40. Thin section views (crossed and uncrossed polars) of the thin section U5-365-b. Field of view = ~ 40 x 25 mm.

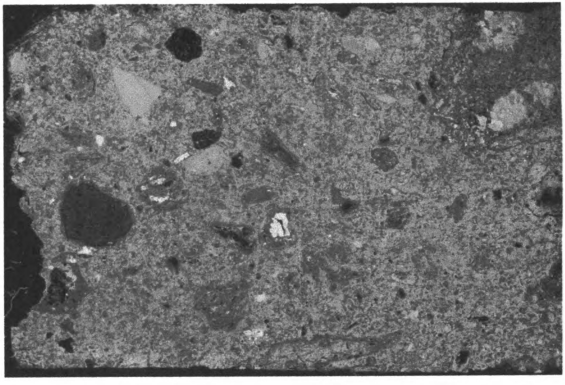

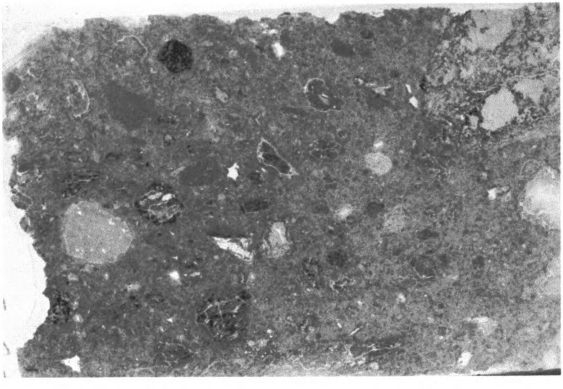

Figure 41. Thin section views (crossed and uncrossed polars) of the thin section U5-383-2a. Field of view = ~ 40 x 25 mm.

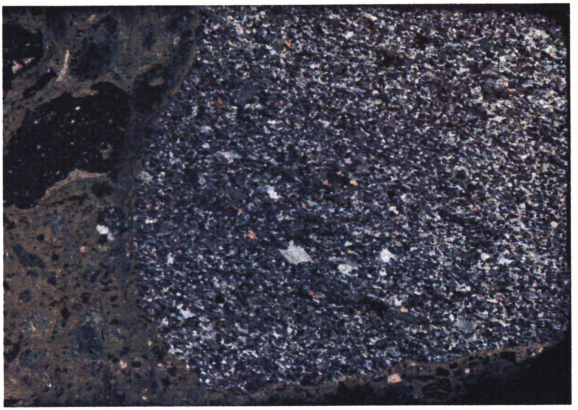

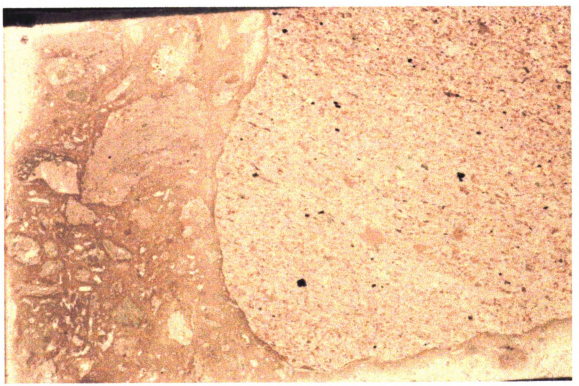

Figure 42. Thin section views (crossed and uncrossed polars) of the thin section U5-400-b. Field of view = ~ 40 x 25 mm.

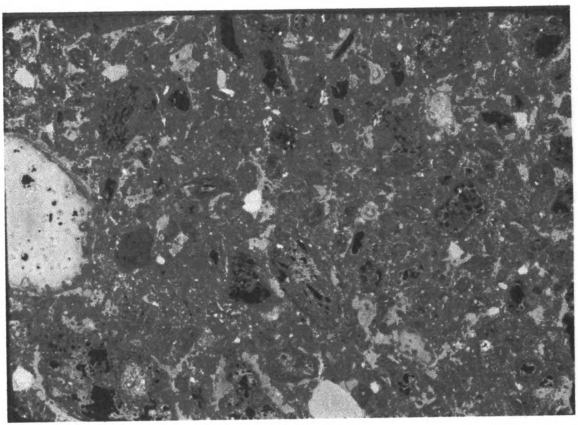

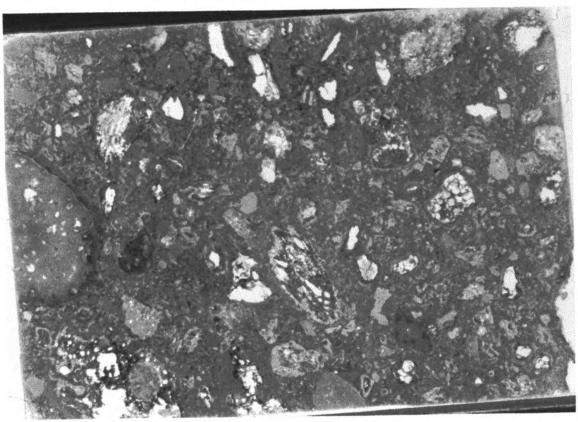

Figure 43. Thin section views (crossed and uncrossed polars) of the thin section U5-420-b. Field of view = ~ 40 x 25 mm.

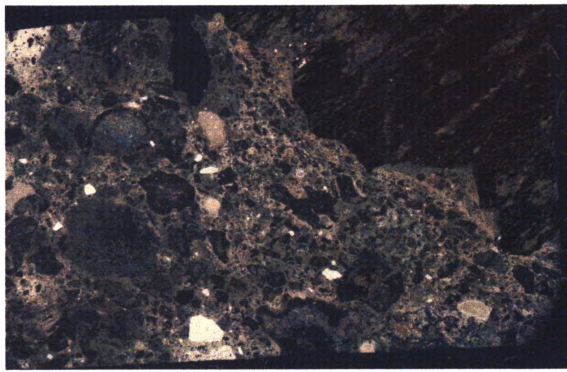

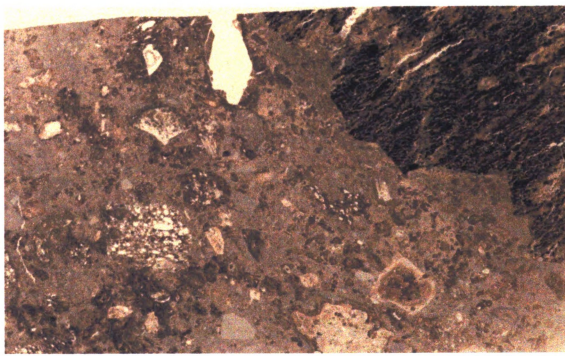

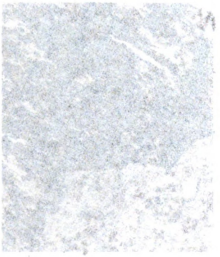

Figure 44. Thin section views (crossed and uncrossed polars) of the thin section U5-450-b. Field of view = ~ 40 x 25 mm.

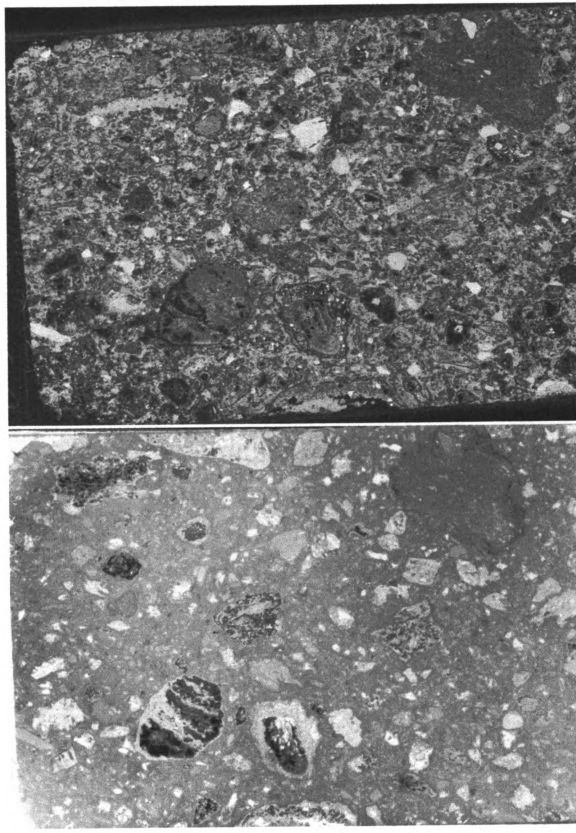

Figure 45. Thin section views (crossed and uncrossed polars) of the thin section U5-483-a. Field of view = ~ 40 x 25 mm.

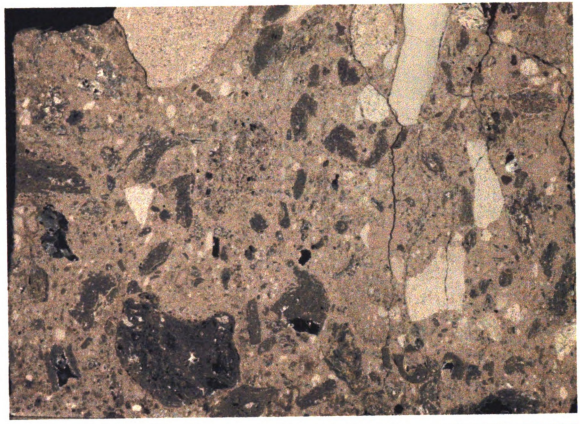

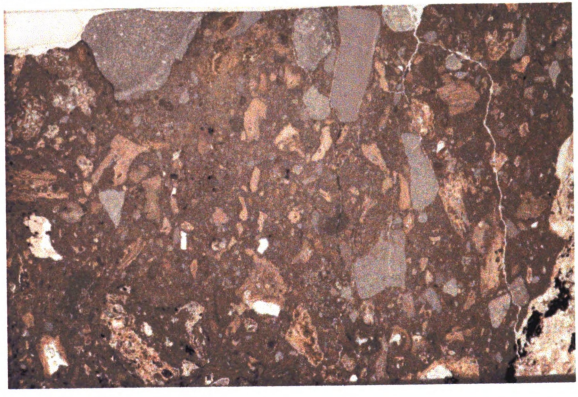

Figure 46. Thin section views (crossed and uncrossed polars) of the thin section U6-302-b. Field of view = ~ 40 x 25 mm.

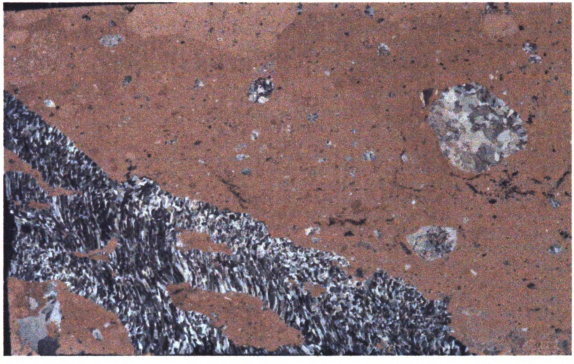

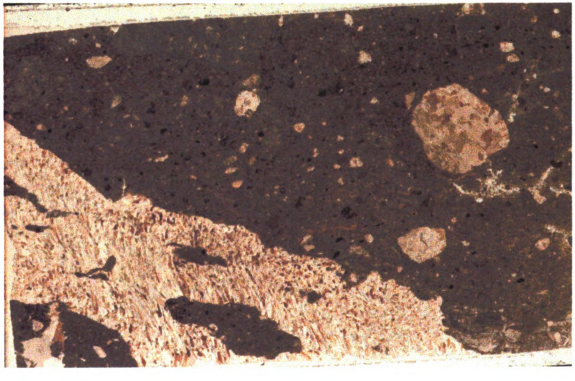

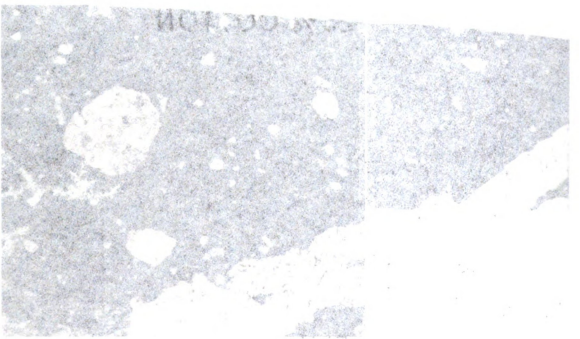

Figure 47. Thin section views (crossed and uncrossed polars) of the thin section U7-335-b. Field of view = ~ 40 x 25 mm.

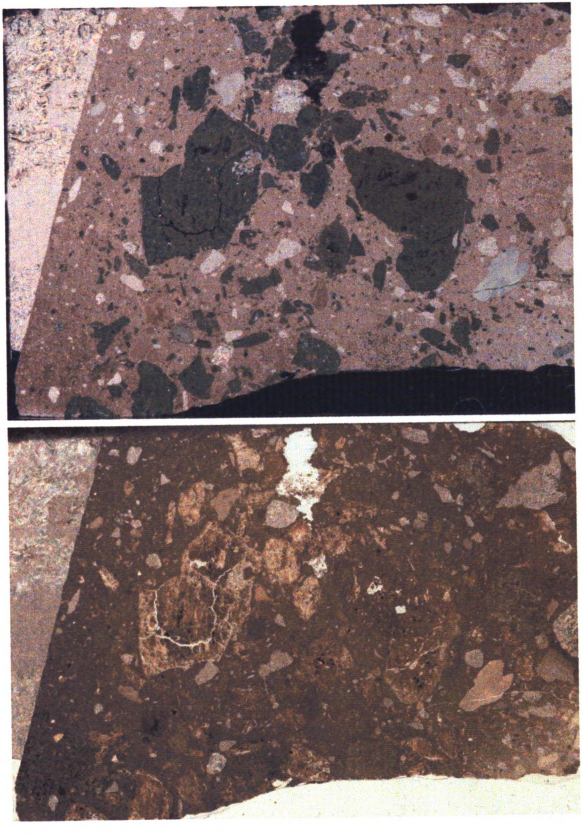

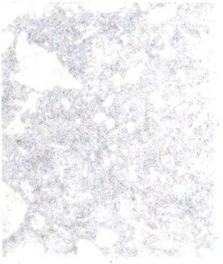

APPENDIX D

Figure 48. Elemental maps corresponding to a breccia boundary in the upper portion of the U5-420-b thin section (Figure 43). Colored scale represents counts. Analyzed element is shown at the bottom of each frame.

500 um BSE1 15kV 20n
500 um Si 15kV 20nA
500 um Ca 15kV 20nA
500 um K 15kV 20nA
500 um Fe 15kV 20nA
500 um Mg 15kV 20nA

Figure 49. Elemental maps corresponding to a breccia boundary in the upper portion of the U5-420-b thin section (Figure 43). Colored scale represents counts. Analyzed element is shown at the bottom of each frame.

500 um BSEI 15kV 20n
500 um Al 15kV 20nA
500 um P 15kV 20nA
500 um S 15kV 20nA
500 um Ti 15kV 20nA
500 um Na 15kV 20nA

Figure 50. Elemental maps corresponding to a breccia boundary in the upper portion of the U5-420-b thin section (Figure 43). Colored scale represents counts. Analyzed element is shown at the bottom of each frame.

500 um BSE1 15kV 20nA
500 um Si 15kV 20nA
500 um Ca 15kV 20nA
500 um K 15kV 20nA
500 um Fe 15kV 20nA
500 um Mg 15kV 20nA

Figure 51. Elemental maps corresponding to a breccia boundary in the upper portion of the U5-420-b thin section (Figure 43). Colored scale represents counts. Analyzed element is shown at the bottom of each frame.

500 um BSE1 15kV 20n
500 um Al 15kV 20nA
500 um P 15kV 20nA
500 um S 15kV 20nA
500 um Ti 15kV 20nA
500 um Na 15kV 20nA

BIBLIOGRAPHY

BIBLIOGRAPHY

Bohor, B. F.,Betterton, W. J., and Krogh, T. E., 1993, Impact-shocked zircons: discovery of shock-induced textures reflecting increasing degrees of shock metamorphism: Earth and Planetary Science Letters, v. 119, p. 419-424.

Buffler, R. T., and Sawyer, D. S., 1985, Distribution of crust and early history, Gulf of Mexico Basin: Gulf Coast Association of Geological Societies Transactions, v. 35, p. 333-344.

Corrigan, C. M., Sharpton, V. L., Vogel, T. A., and Marin, L. E., 1997, Chemical Compositions of Chicxulub Impact Breccias, LPI Contribution No. 922, p. 10-11.

Dietz, R. S., and Holden, J. C., 1970, Reconstruction of Pangea: Breakup and dispersion of continents, Permian to Recent: Journal of Geophysical Research, v. 75, p. 4939-4956.

Dressler, B. O., Grieve, R. A. F., 1994, The Sudbury structure: Constraints on its genesis from Lithoprobe results: Geophysical Research Letters, v. 21, p. 963-966.

Hall, D. J., Cavanaugh, T. D., Watkins, J. S., and McMillen, K. J., 1982, The rotational origin of the Gulf of Mexico based on regional gravity data, *in* Watkins, J. S., and Drake, C. L., eds., Studies in continental margin geology: Amerian Association of Petroleum Geologists Memoir 34, p. 115-126.

Hildebrand, A. R., Penfield, G. T., Kring, D. A., Pilkington, M., Camargo, Z. A., Jacobsen, S. B., and Boynton, W. V., 1991, Chicxulub crater: A possible Cretaceous/Tertiary boundary impact crater on the Yucatán peninsula, Mexico: Geology, v. 19, p. 867-871.

Horz, F., 1982, Ejecta of the Ries Crater, Germany: *in* Silver, L. T., and Schultz, P. H., Geological Implications of Impacts of Large Asteroids and Comets on the Earth; Geological Society of America Special Paper 190, p. 39-55.

Izett, G. A., Dalrymple, G. B., and Snee, L. W., 1991, $^{40}Ar/^{39}Ar$ age of Cretaceous/Tertiary boundary tektites from Haiti: Science v. 252 p. 1539-1542.

Koeberl, C., Sharpton, V. L., Schuraytz, B. C., Shirey, S. B., Blum, J. D., and Marín, L. E., 1994, Evidence for a meteoritic component in impact melt rock from the Chicxulub structure: Geochemica et Cosmochimica Acta, v. 58, p.1679-1684.

Krogh, T. E., Kamo, S. L., and Bohor, B. F., 1993a, Fingerprinting the K/T impact site and determining the time of impact by U-Pb dating of single shocked zircons from distal ejecta: Earth and Planetary Science Letters, v. 119, p. 425-429.

Krogh, T. E., Davis, D. W., and Corfu, F., 1984, Precise U-Pb zircon and baddeleyite ages for the Sudbury area; *in* The geology and ore deposits of the Sudbury Structure, Ontario Geological Survey, Special Volume 1, p. 431-446.

Melosh, H. J., 1989, Impact cratering - A geologic process: New York, OxfordUniversity Press, 245 p.

Mills, J. G. Jr., Saltoun, B. W., and Vogel, T. A., 1997, Magma batches in the Timber Mountain magmatic system, Southwestern Nevada Volcanic Field, Nevada, USA: Journal of Volcanology and Geothermal Research, v. 78, p. 185-208.

Ocampo, A. C., Pope, K. O., and Fischer, A. G., 1996, Ejecta blanket deposits of the Chicxulub crater from Albion Island, Belize: *in* Ryder, G., Fastovsky, D., and Gartner, S., eds., The Cretaceous-Tertiary Event and Other Catastrophes in Earth History; Geological Society of America Special Paper 307, p. 75-88.

Pindell, J. L., 1985, Alleghenian reconstruction and subsequent evolution of the Gulf of Mexico, Bahamas and Proto-Caribbean: Tectonics, v. 4, p. 1-39.

Reimold, W. U., 1994, Hydrothermal Witwatersrand gold mineralization caused by the Vredefort mega-impact event? *in* Conference on new developments regarding the KT event and other catastrophes in Earth history [abs.], LPI Contribution 825, Lunar and Planetary Institute, Houston, p. 92-93.

Ross, M. I., and Scotese, C. R., 1988, A heirarchical tectonic model of the Gulf of Mexico and Caribean region: Tectonophysics, v. 155, p. 139-168.

Salvador, A., 1987, Late Triassic-Jurassic paleogeography and origin of Gulf of Mexico Basin: American Association of Petroleum Geologists Bulletin, v. 71, p. 419-451.

Salvador, A., 1991, Origin and development of the Gulf of Mexico basin, *in* Salvador, A., ed., The Gulf of Mexico Basin: Boulder, Colorado, Geological Society of America, The Geology of North America, v. J., p. 389-444.

Sharpton, V. L., Schuraytz, B. C., Burke, K., Murali, A. V., and Ryder, G., 1990, Detritus in K/T boundary clays in western North America; Evidence against a single oceanic impact, in Sharpton V. L., and Ward, P. D., eds., Global catastrophes in Earth history; An interdisciplinary conference on impacts, volcanism, and mass mortality; Geological Society of America Special Paper 247, p. 349-357.

Sharpton, V. L., Dalrymple, G. B., Marín, L. E., Ryder, G., Schuraytz, B. C., and Urrutia-Fucugauchi, J., 1992, New links between the Chicxulub impact structure and the Cretaceous/Tertiary boundary: Nature, v. 359, p. 819-821.

Sharpton, V. L., Burke, K., Camargo-Zanoguera, A., Hall, S. A., Lee, S., Marin, L. E., Suarez-Reynoso, G., Quezada-Muneton, J. M., Spudis, P. D., and Urrutia-Fucugauchi, J., 1993, Chicxulub multi-ring impact basin: Size and other characteristics derived from gravity analysis: Science, v. 261, p. 1564-1567.

Sharpton, V. L., Marín, L. E., Carney, J. L., Lee, S., Ryder, G., Schuraytz, B. C., Sikora, P., and Spudis, P. D., 1996, A model of the Chicxulub impact basin based on evaluation of geophysical data, well logs, and drill core samples: *in* Ryder, G., Fastovsky, D., and Gartner, S., eds., The Cretaceous-Tertiary Event and Other Catastrophes in Earth History; Geological Society of America Special Paper 307, p. 55-74.

Sharpton, V. L., 1997, Surface expression of the Chicxulub crater; Comment and Reply: Geology, v. 25, p. 567-568.

Sharpton, V. L., Corrigan, C. M., Dressler, B. O., Marin, L. E., Urrutia, J., and Vogel, T. A., 1998, Nature and Composition of Impact Produced Breccias along the Southern Flank of the Chicxulub Basin: in preparation.

Spudis, P. D., 1993, The geology of multi-ring impact basins: Cambridge, England, Cambridge University Press, 263 p.

Swisher, C. C., III, Grajales-Nishimura, J. M., Montanari, A., Margolis, S. V., Claeys, P., Alvarez, W., Renne, P., Cedillo-Pardo, E., Maurrasse, F. J-M. R., Curtis, G. H., Smit, J., and McWilliams, M. O., 1992, Coeval $^{40}Ar/^{39}Ar$ ages of 65.0 million years ago from Chicxulub crater melt rock and Cretaceous-Tertiary boundary tektites: Science, v. 257, p. 954-958.

Urrutia-Fucugauchi J., Marín, L., and Sharpton, V. L., 1994, Reverse polarity magnetized melt rocks from the Cretaceous/Tertiary Chicxulub structure, Yucatán peninsula, Mexico: Tectonophysics, v. 237, p. 105-112.